

Received 11 July 2023, accepted 24 July 2023, date of publication 27 July 2023, date of current version 2 August 2023.

Digital Object Identifier 10.1109/ACCESS.2023.3299290

 SURVEY

# Research on GNSS INS & GNSS/INS Integrated Navigation Method for Autonomous Vehicles: A Survey

YUAN HE<sup>1</sup>, JICHUAN LI<sup>2</sup>, AND JUNJIE LIU<sup>2</sup>

<sup>1</sup>School of Natural Science, Anhui Agricultural University, Hefei 230036, China

<sup>2</sup>Beijing Institute of Remote Sensing Equipment, Beijing 100854, China

Corresponding author: Yuan He (yuanhe2023@126.com)


This work was supported in part by the National Natural Science Foundation of China under Grant 61431004, Grant G051917003, and Grant 11774074.

**ABSTRACT** Autonomous Vehicles have become the focus of research around the world. Meanwhile, the continuous development of various emerging technologies in recent years has paved the way for the realization of fully autonomous driving. Furthermore, high-precision navigation and positioning systems are crucial to self-driving cars. For navigation and positioning technology of autonomous vehicles, Global Navigation Satellite System (GNSS)/Inertial Navigation System (INS) integrated navigation is of great significance to realizing high-precision navigation and positioning of autonomous vehicles. This paper researches and summarizes the development and current situation of GNSS, INS, and GNSS/INS integrated navigation technology. GNSS/INS integrated navigation algorithms are divided into four different models of combination methods: Ultra tightly Coupled, Tightly Coupled, Semi-tightly Coupled, and Loosely Coupled. Besides, the advantages and disadvantages of these four integrated navigation algorithms are compared and discussed. The characteristics of different GNSS/INS coupling models are summarized in the last chapter, and the potential research direction of GNSS/INS in the future is proposed.

**INDEX TERMS** Autonomous vehicles, Global Navigation Satellite System, inertial navigation system, GNSS/INS integrated navigation.

## I. INTRODUCTION

Positioning and navigation technology contain abundant social functions and substantial economic benefits, playing an indispensable role in every field of society. Achieving high-precision navigation and positioning is increasingly essential in this rapid autonomous driving development era. To improve the safety and efficiency of transportation, improving the positioning methods to perform high-precision positioning of vehicles is needed [1], [2], [3], [4], [5], [6], [7], [8]. Compared with Global Positioning System (GPS), the Global Navigation Satellite System (GNSS) has the advantages of low cost, high accuracy, and no accumulation of positioning errors with time. These advantages can improve the observation ability by getting correlative observations and eliminating errors.

The associate editor coordinating the review of this manuscript and approving it for publication was Junho Hong .

Inertial Navigation System (INS) can obtain the navigation parameters such as three-dimensional (3D) velocity, position, and attitude information through their gyros and accelerometers. Their positioning accuracy will not be affected by the exogenous environment. However, GNSS has some problems, such as the signal being easily blocked in the moving state, low data update rate, and poor reliability in the dynamic environment. INS positioning errors accumulate continuously over time. Thus, the integrated navigation of GNSS/INS can complement each other and improve the system's overall navigation accuracy and reliability. Therefore, GNSS/INS integrated navigation technology is crucial to high-precision automatic driving positioning.

Nowadays, GNSS mainly includes four typical satellite navigation systems: GPS, Galileo, GLONASS, and Beidou navigation satellite system (BDS) [9], [10], [11], [12], [13], which particularly realize the function of real-time

positioning of objects. Beidou-2 navigation satellite system (BDS-2). Beidou-3 navigation satellite system (BDS-3). Theoretically, when the distance between satellite and target, satellite coordinate, and satellite clock error is known, the target coordinate can be calculated by GNSS observation value and basic observation equation. Still, the actual electromagnetic wave transmission will be affected by the relativistic effect, ionospheric error, tropospheric error, and multipath effect. So it is necessary to use the model to eliminate the influence of error and calculate the accurate target coordinate.

To solve these problems, an optimized GNSS multipath elimination method Advanced Trend surface analysis-based Multipath Hemispherical Model (AT-MHM) is now adopted. This method is extended to double-difference (DD) mode, which expands the scope of the application. AT-MHM has strong noise resistance and solves the overfitting problem caused by multipath anisotropy [14].

However, suppose the distance is far or the target object is moving. In that case, the satellite signal power level is reduced, and the accuracy of the satellite's position, velocity, and time would also be reduced [5], [15], [16], [17], [18], [19], [20]. When an automatic driving vehicle is moving, the positioning accuracy of GNSS will be affected. This may lead to the failure to reach the destination timely and accurately. In INS, the Inertial Measurement Unit (IMU) can measure the three-axis angular velocities and three-axis accelerations of the current vehicle and calculate the speed and position of the object in the navigation coordinate system. It will not be affected by signal transmission and has high stability. However, the high-precision INS system is expensive, which leads to an increase in the cost of the automatic driving system. The low-precision INS system is inadequate to meet the requirements of positioning accuracy. Therefore, an automatic navigation and positioning method with high precision and low cost is needed.

The existing GNSS/INS integrated method adopts the optimal estimation algorithm based on Kalman Filter (KF). This algorithm fuses GNSS and INS positioning and navigation information and combines them with KF [18], [21], [22], [23], [24], [25], [26] to estimate and eliminate the errors of INS system speed, position, and attitude. The adaptive Kalman filter (AKF) integral [27], [28], [29], [30], [31], [32], [33] achieves long-term and stable high-precision positioning. The analysis demonstrates that the combination can generate high-frequency navigation information. It can maintain high precision and low cost in long and short-term navigation. It also can promote the popularization of high-precision and low-cost automatic driving navigation systems and solve the high-precision positioning problem of the automatic driving system.

Although the GNSS/INS integrated navigation technology is very mature, cars continue to travel in more complex environments (underground tunnels, viaducts, woods, and tall buildings). The signal is easily blocked in a complex environment, resulting in low positioning accuracy. Therefore,

positioning and navigation technology must be continuously researched and updated for the constantly changing driving environment. In recent years, many GNSS/INS optimization combination methods have emerged. For example, the accuracy of the GNSS/INS integrated algorithm is affected by the pitch and heading mounting angles of IMU in INS. Therefore, the Dead Reckonings (DR) approach utilizes the integrated attitude and distance traveled of GNSS/INS to estimate IMU mounting angles. The integrated position fusion of DR and GNSS/INS is adopted to improve positioning accuracy [34], [35], [36], [37]. Due to INS being expensive, a low-cost, simple inertial sensor system, the Reduced Inertial Sensor System (RISS), is proposed to work with Precise Point Positioning (PPP).

On the one hand, the Tightly Coupled (TC) integration mode is selected, and PPP network error model correction is used. On the other hand, the difference between the predicted value and the measured value of GNSS is taken as a measurement error by Extended KF (EKF). The filter fuses systematic errors and measurement errors to generate the final estimated position, velocity, and attitude [38], [39], [40], [41], [42]. Research and development of autonomous vehicles would become a global trend, and automatic driving technology would significantly improve the efficiency, convenience, and safety of the whole road and traffic systems [43], [44], [45], [46], [47], [48]. Therefore, the development and current situation of GNSS, INS, and GNSS/INS integrated navigation technology are studied and summarized in this paper. The writing motivation of our paper is to enable scholars to quickly understand the development and current situation of GNSS/INS integrated navigation. A comprehensive review of the typical developments of GNSS, INS, and GNSS/INS integrated navigation is the main content of this paper. Our paper is organized as follows: In Section II, we summarize a large number of research on autonomous navigation and positioning technology and briefly present the development history of autonomous vehicles navigation and positioning technology from GNSS to GNSS/INS integrated navigation. In Section III, we give a detailed summary of the development status of GNSS and INS, respectively. In Section IV, the listed GNSS/INS integrated navigation algorithms are divided into four categories: Ultra-tightly Coupled, Tightly Coupled, Semi-tightly Coupled, and Loosely Coupled, elaborating the specific content of these algorithms in detail. In Section V, we compare and analyze the listed GNSS/INS integrated navigation algorithms and summarize the characteristics of different algorithms. The potential future research directions of GNSS/INS integrated navigation have been prospected as follows.

## II. APPLICATION PROGRESS IN AUTONOMOUS VEHICLE OF GNSS AND GNSS/INS

Automatic driving mainly involves three aspects: positioning, perception, and planning control. This paper specifically discusses the development of automatic driving positioning. Since the mid-1980s, GPS has provided a foundation for

automatic driving positioning technology, promoting the development of automatic driving [49]. In 1995, Schönberg et al. discussed the fusion of internal dead reckoning navigation and periodic absolute position measurements and used Differential GPS (DGPS) in experiments of unmanned cars [50]. In the same year, Hermann et al. put forward the On-The-Fly (OTF) GPS positioning algorithm to accurately determine the vector between GPS antennas and evaluated the positioning capability of the OTF algorithm. The results demonstrate that the OTF algorithm could be used for relative motion positioning and achieve high-precision vehicle positioning [51].

In the 21st century, due to the increasingly complex driving environment, automatic positioning technology has gradually developed from GNSS to GNSS/INS integrated. In 2010, Angrisano et al. researched GNSS/INS integrated navigation, pointing out that GNSS can no longer achieve continuous and stable positioning in urban areas, and tried different GNSS/INS integrated methods [52]. In the same year, Liu et al. proposed using Rauch Tung Striebel Smoothens (RTSS) algorithm to improve the accuracy of Land-Vehicle Navigation (LVN) to solve the loss of GPS signals and rapid increase of INS errors with time in urban navigation [53]. In 2016, Lombard et al. proposed a steering wheel angle control algorithm that adapts to the speed of the car. This algorithm can achieve the goal that the driverless car's curve and straight line work by simultaneously controlling the vehicle's steering wheel angle and acceleration. And realizing the flexible driving of the self-driving car [54]. Zhang et al. aiming at the problems of GNSS data delay and long solution time of integrated update in GNSS/INS tight integrated navigation system, proposed a KF mathematical model which transfers the error state vector to the current moment in one step after completing the delayed observation update. Compared with the standard Kalman model, this model has the same navigation accuracy, but the delay in outputting navigation results is less, which ensures the real-time performance of integrated navigation results [55]. In 2018, Wang et al. adopted Allan Variance (AV) analysis technology instead of the general auto-regressive processes to establish an error model. Their results demonstrated that the overall accuracy of the combined algorithm combined with Differential GNSS (DGNSS) was 18%, 8%, and 38%, higher than that of the traditional algorithm in position, velocity, and attitude, respectively. The overall accuracy combined with Single Point Positioning (SPP) was 15%, 75%, and 77% higher than that of the traditional algorithm in position, velocity, and attitude, respectively, which significantly improves the positioning accuracy of the vehicle [56]. In the same year, Lyu et al. proposed a vehicle-borne jammer detection and location algorithm based on binary tree Support Vector Machine (SVM) classification technology. The algorithm was tested in urban canyons and residential areas, respectively. The conclusion is that when the training data set covers the interference signal characteristics, the correct localization

rate can reach more than 90%. The average positioning error can be less than 30 m. The algorithm can continuously enrich the training data set and improve the positioning performance through learning, which has reference significance for realizing the high-precision positioning of unmanned vehicles [57].

Ning et al. aiming the dynamic error and observation of gross error of GNSS/INS loose coupling, an optimal Radial Basis Function (RBF) neural network-enhanced adaptive robust KF method was proposed to reduce the influence of errors. Firstly, the method took the test statistics of Mahalanobis distance as the judgment index to realize fault detection and used the optimal principle to train an optimal RBF neural network strategy online. Experiments demonstrate that this method's two error elimination rates for the complex urban environment were 92% [58]. Li et al. from Tsinghua University proposed a reliable and high-precision TC Real-time kinematic (RTK)/INS algorithm, which was not affected by cycle slips and large pseudo-range noises. It had better stability and higher accuracy than RTK and the traditional RTK/INS close-coupling method [37]. In 2019, Wei Jiang et al. proposed a vehicle navigation system integrating GNSS, INS, and Optical Velocity Sensors (OVS). In this system, the measured value of GNSS, the pseudo-range and pseudo-range rate difference derived from INS, and the velocity difference derived from INS and OVS were used as the measurement input of the system filter to obtain an accurate navigation solution. The fault-tolerant Fault Detection and Processing (FDP) algorithm was used to detect the fault. The results demonstrate that the accuracy of the integrated system was higher than that of the Loosely Coupled system algorithm and had significant advantages in fault tolerance and accuracy [59]. In the same year, Elsheikh et al. proposed to combine real-time Single-Frequency Precise Point Positioning (SF-PPP) with low-cost INS to provide continuous and accurate navigation solutions for the problem of low positioning accuracy of GNSS SF-PPP due to frequent signal degradation and blocking. The test results demonstrate that the PPP/INS system could maintain the horizontal sub-meter Root Mean Square (RMS) accuracy in outdoor and suburban environments [60]. In 2021, Li et al. proposed a semi-tight coupling mode of multi GNSS PPP and Stereo Visual Inertial Navigation Systems (S-VINS), which realized the data sharing between the two navigation systems, and significantly improved the vehicle positioning ability. The data demonstrate that the 3D positioning accuracy of GPS, GPS+GLOANSS, GPS+, and GPS+GLOANSS+BDS was 49.0%, 40.3%, 45.6%, and 51.2%, which was higher than the original solution. The semi-tight coupling model of Multi-GNSS PPP/S-VINS 3D positioning accuracy had been improved by 41.8-60.6% compared with multi GNSS PPP/INS [61].

This section discusses the application and development of GNSS/INS Integrated Navigation in automatic driving. TABLE 1 demonstrates some cases of GNSS/INS integrated

**TABLE 1. Classical algorithms for GNSS/INS integrated navigation.**

Method	Accuracy	Situation	Availability	Combination Model
A Tightly Coupled RTK/INS Algorithm with Ambiguity Resolution [37]	Good	In experiment	Partly	Tightly Coupled
A Fault-Tolerant Tightly Coupled GNSS/INS/OVS Integration [59]	Good	In experiment	Partly	Tightly Coupled
Low-Cost Real-Time PPP/INS Integration [60]	Unknown	In experiment	Partly	Unknown
Semi-tightly Coupled integration of multi GNSS PPP and S-VINS [61]	Good	In experiment	Partly	Semi-tightly Coupled
INS/GNSS/Light Detection and Ranging (LiDAR) Simultaneous Localization and Mapping (SLAM) [62]	Good	In experiment	Partly	Unknown
An Improved Single-epoch GNSS/INS [63]	Good	In experiment	Partly	Tightly Coupled
A Novel Linear Model GNSS/INS [64]	Unknown	In experiment	Partly	Ultra-tightly Coupled
GNSS/INS/Vehicle Dynamic Models (VDM) [65]	Unknown	In theory	Partly	Unknown
Spoofing Detection Using GNSS/INS/Odometer (OD) Coupling [66]	Unknown	In experiment	Partly	Unknown
TC Positioning by GPS/BDS-2/BDS-3/INS [67]	Good	In experiment	Partly	Tightly Coupled

navigation. According to the indicators in the table, it can be seen that the positioning accuracy of the above-integrated navigation has been significantly improved compared with GNSS, and the positioning error is also reduced [68], which is of great significance for the realization of high-precision positioning of unmanned vehicles. These combinations are different modes, and the different coupling degrees would inevitably affect the accuracy. For example, the combination in [64] adopts an ultra-tight combination, so the accuracy of the combination would be improved compared with other TC modes. However, analyzing the table carefully reveals that all varieties have some usability flaws that need to be improved. Synthesizing the above analysis, realizing the high-precision positioning of the automatic driving vehicle remains a complex problem. The application of GNSS/INS Integrated Navigation in automatic driving still needs to be investigated through continuous experiments in the future. At the same time, real-time fault detection of GNSS/INS integrated navigation is necessary [56], [69], [70], [71], [72], [73] to improve the stability of system operation and adapt to the rapid development of automatic driving.

The second section introduces the general application of GNSS and GNSS/INS in automatic driving in recent twenty years.

### III. A DETAILED RESEARCH OF GNSS AND INS RESPECTIVE TECHNICAL DEVELOPMENT PROCESS

Through browsing the above parts of the article, it could be seen that the development background and history of GNSS/INS integrated navigation, understanding of the development of GNSS/INS integrated navigation. To let scholars have a deeper understanding of integrated navigation at the level of technical methods, this section screens out the typical cases that can reflect the development of GNSS and INS in the last 20 years. It summarizes them from the technical level so that scholars can quickly understand the development status of GNSS and INS.

#### A. CLASSICAL ALGORITHM OF GNSS

Aiming at the multipath effect of GNSS carrier phase data affecting the final positioning accuracy, a ray-tracing method was proposed to eliminate the multipath error [74]. The known geometry of the satellite reflector antenna is used to

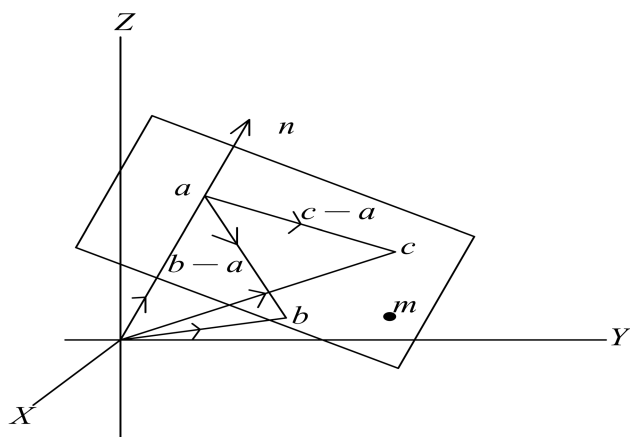


FIGURE 1. The vector equation of a plane [74].

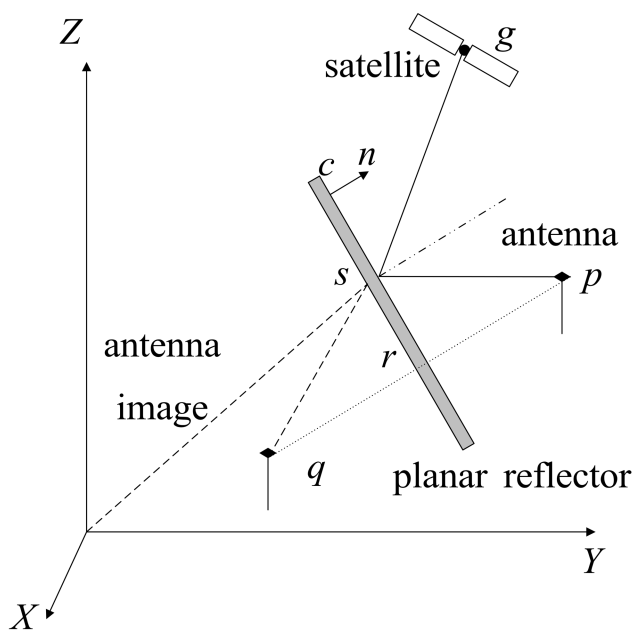


FIGURE 2. The geometry of the intersection of a line and a plane [74].

estimate the number of multipath to correct the multipath error of GNSS carrier phase data. To establish the multipath estimation model, it is necessary to understand the geometric principle of ray tracks. That is using the vector method to determine the plane equation (Fig. 1 to determine the reflection surface) and the intersection point of the line and plane (Fig. 2 to trace the rays transmitted from the satellite through the reflection surface to reach the antenna).

As demonstrated in Fig. 1,  $n$  is the normal vector of the plane. To determine whether the given point of  $m$  is on the plane, it only needs to determine whether the dot product of the vector of  $(m-a)$  and  $n$  is 0. As demonstrated in Fig. 2, the nearest point  $r$  to antenna  $p$  should be found first. The position difference vector  $(r-p)$  should be calculated to estimate the multipath possibility of satellite signals. Then,

it is necessary to find the antenna image position  $q$  and determine the line between  $s$  and  $g$ ,  $s$  and  $q$ . Finally, according to the position of the four corners of the reflective surface, it is necessary to judge whether  $s$  is located on the reflective surface. By knowing the geometry of the reflecting surface, reflecting process, antenna type, and the whole multipath process of receiver tracking loop to determine the influencing factors (relative permittivity of the reflector, incidence angles, polarization efficiency state, correlator spacing, the distance between the receiving antenna and the Reflector, a wavelength of the carrier) of multipath error characteristics in GNSS carrier phase measurement. Reference [74] developed a GNSS carrier phase data simulator successfully, which can generate multipath error characteristics, and compared the experimental multipath error of GPS signal under three conditions of metal, water, and brick building with the model multipath error. The actual value of the steel plate reflection experiment was consistent with the predicted value, with a slight difference of only 2-5 mm. It is difficult for the water surface experiment simulator to imitate the reflection condition of the water surface at any time. Still, the law of multipath amplitude and frequency changing with time is summarized. A suitable alignment exists between the amplitude of the actual value and the predicted value of the brick house reflection experiment.

In the research of ionospheric time delay prediction, [75] proposed to use of the linear time series model and Autoregressive and Moving Average (ARMA)-based ionospheric Total Electron Content (TEC) multivariate prediction model to predict the ionospheric changes to achieve good satellite navigation. The model is divided into two parts: linear and ARMA predictions. This paper uses the 8-year GPS data of the 24th solar activity cycle of the Bengaluru GNSS station for experiments. Geomagnetic activity, extreme ultraviolet (EUV) irradiance, and periodic oscillation are taken as the model's input parameters. Firstly, the ionospheric linear TEC model considers the factors such as periodic oscillation, solar EUV irradiance, and geomagnetic activity and adopts hourly Vertical Total Electron Content (VTEC) value to improve the model's performance in short-term and long-term changes in the estimated area. Secondly, ARMA is a time series and prediction model, which is usually a traditional short-term and long-term TEC prediction model and is suitable for estimating the spatial changes of the ionosphere under geomagnetic disturbance and static conditions. The past prediction residuals and Moving average (MA) components of this model will affect the performance of this model.

Aiming at the problem of satellite failure caused by the multipath effect and Non-Line-Of-Sight (NLOS), [76] proposed using consistency check to detect and eliminate failed satellites, to realize high-precision positioning of automobiles. This study uses two multi-fault detections and exclusion (FDE) algorithms (exhaustive and greedy searches). Exhaustive searches and greedy searches respectively represent the theoretical and practical performance of FDE based on consistency test. In exhaustive searches, if the

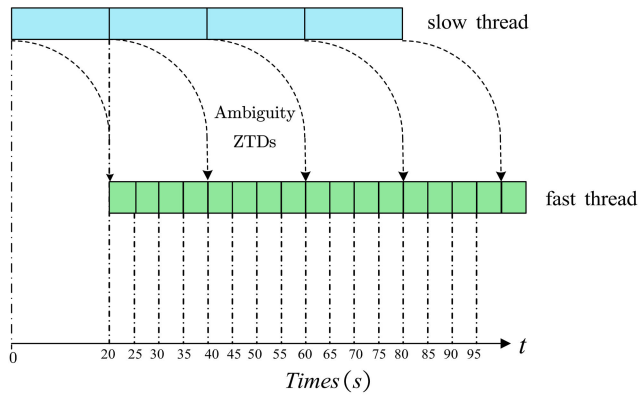


FIGURE 3. Dual-thread parallel real-time clock estimation algorithm [78].

satellite calculation test statistics in the view can't pass the chi-square test, one or more satellites must be excluded to find the healthy measurement value. Greedy search for the optimal solution circularly or locally, assuming only one polluted satellite. If the satellite calculation test statistics in the view cannot pass the chi-square test, a subset will be generated, and one of the surviving satellites will be excluded. If multiple subsets pass the second fault detection, the subset with the smallest test statistics is selected. The original data of the GNSS experiment and the actual ground data provided by the SIP-Ades project are used in [76] to conduct experiments and to evaluate the performance of the two algorithms in urban canyons. The experimental results demonstrate that the FDE based on the greedy algorithm can achieve good positioning in the central valley of the city, and both the exhaustive and greedy searches can achieve sub-meter average lateral positioning accuracy. But the lateral errors of the two FDE are more than 10 meters for deeper urban canyons.

To solve the problems of low-cost GNSS poor accuracy and inconvenient use in urban areas, [77] proposed to apply the EKF system to fuse the absolute positioning data of low-cost GNSS receiver with the relative data of four-wheel speed sensors, a steering wheel angle sensor, and a lateral acceleration sensor, to realize the high-precision positioning of vehicles during GNSS interruption. Firstly, the system extracts the original data from all sensors, and then it will need preprocessing to convert these data into meaningful variables. The next step is data fusion. The preprocessing results are input into the EKF refined by the bicycle kinematics model and Ackerman steering geometry model to realize the best estimation of the output system. It is concluded through experiments that the positioning accuracy of GNSS receivers with a lower cost of this system is improved. The accuracy of Root Mean Square Error (RMSE) can be increased by 50%. The 95th-percentile of the distance error distribution is increased by 50%, and the maximum distance error is increased by 75%.

To solve the problem, the traditional undifferenced (UD) clock estimation method is inefficient and cannot meet the

demand of multi-constellation GNSS (multi-GNSS) real-time clock estimation. Reference [78] proposed a dual-thread parallel algorithm composed of two threads with different computational efficiency. It was applied to multi-GNSS real-time clock estimation to meet the demand for multi-GNSS real-time PPP technology. At present, real-time clock estimation methods are divided into the UD method, Epoch-Differenced (ED) method, and Mixed-Differenced (MD) method [79]. The UD method uses UD observations to estimate unknowns. The ED method eliminated the ambiguity by the difference of observation values between two consecutive periods. The MD method should combine these two methods: ED phase observation and UD code observation. As demonstrated in Fig. 3, the slow thread of the dual-thread parallel algorithm adopts the traditional UD method, and it usually takes a long step to update the receiver clock, ambiguity parameters, and satellites. By analyzing the multi-GNSS data of 75 Multi-GNSS Experiment, International GNSS Service, and Crustal Movement Observation Network of China stations, it was verified that the dual-thread parallel algorithm estimates the clock of multi-GNSS. Its clock accuracy is basically the same as the UD method, and its efficiency is much faster than the ED method.

With the rapid development of satellite navigation systems, satellites have realized the transmission of multi-frequency signals. In the research of multi-system data integration, [80] proposed a multi-GNSS triple-frequency PPP model based on non-combined observation to realize multi-system data integration. When the third frequency was introduced into the PPP model, a particular linear combination should be selected. A new inter-frequency deviation was generally adopted to compensate for the pseudo-hardware delay on the third frequency of the model. Reference [80] used GALILEO-only PPP, BeiDou-only PPP, and GPS/GALILEO/BDS PPP. The experimental results demonstrate that the triple-band PPP model has better positioning results than the dual-band PPP model because of the slight delay amplitude of the time-related phase hardware in GALILEO and BDS. In the dynamic mode, the 3D positioning accuracy decreased by 58.17%, 71.50%, and 59.95%, respectively.

To solve the problem of GPS data fusion precision reduction and position jump caused by the multipath effect, [81] proposed a particle weighting Monte Carlo Localization (MCL) model integrating GPS measurement data to solve the problem of GPS data fusion precision reduction. The MCL method is a localization algorithm that combines different sensors [82]. This method is based on a particle filter, and samples are weighted according to the likelihood calculated from available devices [83]. Compare these two methods based on Adaptive Monte Carlo Localization (AMCL), which combines GPS/IMU and LiDAR measurement. These results demonstrate that if the GPS measurement accuracy is low, the particles added by MCL would generate clusters, thus realizing the correct positioning of the vehicle.

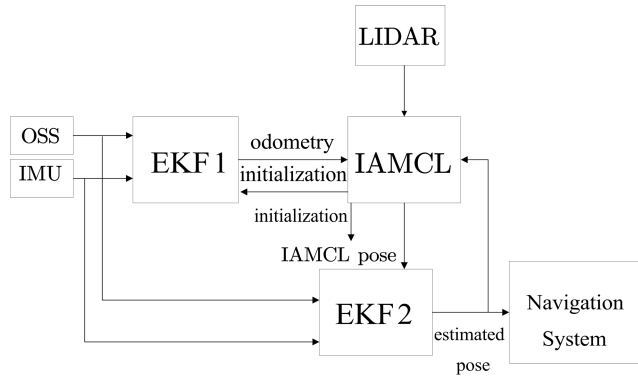


FIGURE 4. Integrated navigation structure diagram [84].

In the research of GNSS-free high-precision positioning of self-driving vehicles, [84] used two EKFs and a particle filter to match lidar scanning. It solves the positioning problem of self-driving vehicles without GNSS. As demonstrated in Fig. 4, this equipment provides accurate speed and direction estimation for Informed Adaptive Monte Carlo Localization (IAMCL). It adopts a simple one-wheel model [85]. IAMCL realizes the estimation of the absolute attitude of an automobile and the processing of an offline map by lidar. EKF2 provides high-frequency and smooth pose estimation for automobiles. The experimental results demonstrate that this method has high stability in avoiding robot abduction in particle filter positioning, and the pose estimation meets the requirements of stability and high speed. The lateral average attitude error ranges from 0.1 m (60 km/h) to 1.48 m (200 km/h), and the longitudinal average ranges from 1.9 m (100 km/h) to 4.92 m (200 km/h).

A probabilistic laser positioning method based on an improved MCL algorithm is proposed in [86], which increases the particle weight by adding GNSS information in the Kalman filter to achieve high-precision positioning of autonomous vehicles. The method in [86] continuously uses GNSS data. By changing the weight of particles and trying to inject new particles, the problem of robot freezing problem can be avoided. In this method, several parameters of two positioning sources are considered. The stability of the particle filter is kept, and the direction error is considered. The method is based on the original adaptive AMCL algorithm. Add GNSS data to the loop, carrying out LiDAR Likelihood, GNSS likelihood estimation, new particle weight calculation, and other steps. Finally, it generates new particles. The experimental results demonstrate that this new automatic driving positioning technology can achieve a good positioning effect in urban and suburban environments. It provides a solution for applying low-cost sensors in different complex environments.

Because of the complexity of autonomous navigation of unmanned vehicles caused by the easy occlusion of GNSS signals in the complex environment of forest, [87] proposed a state estimator combining GNSS, Attitude and Heading Reference Systems (AHRS), and odometry based on LiDAR

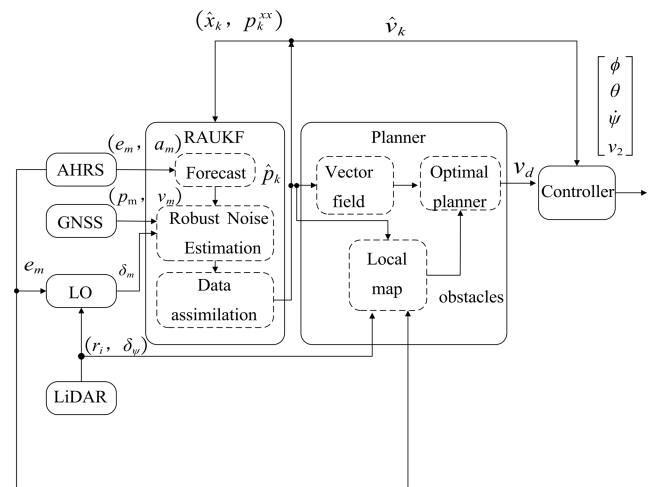
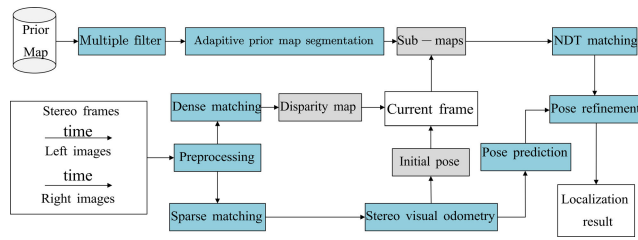


FIGURE 5. Block diagram of the proposed navigation solution [87].

sensors to solve the positioning problem. In the LiDAR-based odometry solution, the relative motion of vehicles is estimated by the trunks of the trees. This method adopts a robust adaptive fusion algorithm based on an unscented Kalman filter. The vector field is combined with the optimal probabilistic planner regarding vehicle motion control. The navigation scheme diagram is demonstrated in Fig. 5. The sensors' data are combined with a robust and adaptive version of Unscented KF (UKF), which outputs and estimates the position and speed of the sensor. The controller's output is micro-aerial vehicle (MAV) roll  $\phi$ , pitch  $\theta$ , yaw rate  $\dot{\psi}$ , and vertical velocity  $v_z$ . The experimental results demonstrate that the multi-sensor fusion algorithm proposed in [87] fully considers the global and relative measurement values. It dramatically improves the navigation and positioning accuracy of automatic vehicles.

Aiming at the phenomenon of error accumulation in long-term operation caused by the lack of loop optimization and prior constraints of the visual and LiDAR SLAM methods, [88] proposed a positioning method with prior dense visual point cloud map constraints generated by a stereo camera. The method is demonstrated in Fig. 6. In the preprocessing, the internal parameters of a stereo camera are calibrated, and stereo images are rectified. Prior visual point cloud maps are obtained by reconstructing the three-dimensional surface of the vehicle-mounted large-scale street. LiDAR is only used for pose estimation in prior visual point cloud map generation. The classical Semi-Global-Block-Matching (SGBM) algorithm estimates the visual point cloud, and the current visual point cloud is initially estimated by stereo visual odometry. The current visual point cloud frame is matched with the candidate sub-map by Normal Distribution Transformation (NDT). Finally, the pose prediction is updated by using the matching result. The experimental results demonstrate that the method proposed in [88] overcomes the problem that the error can easily accumulate due to the lack of loop optimization and



**FIGURE 6.** The proposed pipeline of autonomous vehicle localization [88].

long-term operation. This method can achieve autonomous vehicle positioning without the constraint of GNSS and prior visual point cloud. However, due to the strong dependence on the original visual point cloud, this method is challenging to achieve high-precision positioning when the environmental changes significantly.

**B. CLASSICAL ALGORITHM OF INS**

Aiming at the non-orthogonal frame angle of rotary inertial navigation system affected by the attitude output accuracy, [89] proposed a self-calibration method of non-orthogonal frame angle in three-axis rotary INS (RINS) to improve the attitude output accuracy of RINS. It can improve the navigation accuracy of INS. The measurement parameters of this method are attitude error and velocity error. Three non-orthogonal angles and coupling errors are needed to be calibrated. As demonstrated in Fig. 7, the self-calibration scheme of non-orthogonal angles in tri-axis RINS is divided into two steps. In step 1, the inner and outer gimbal is locked at zero, and the middle gimbal rotates clockwise and counter-clockwise for 180°. When each rotation is completed, the middle gimbal is locked for several minutes. In step 2, the inner and middle gimbal is locked at zero, and the outer gimbal rotates clockwise and counterclockwise for 180°. The duration is less than 30 minutes without external equipment. IMU error, frame rotation axis error, and frame non-orthogonal error are the crucial factors affecting the attitude output accuracy of RINS. IMU error can be self-calibrated based on navigation [90], [91], [92], [93], [94], [95], and frame rotation axis error can use [96]. But frame non-orthogonal error can significantly impact attitude accuracy, so the method of [89] can be adopted. The actual triaxial RINS results demonstrate that the method in [89] can make the non-orthogonal angle accuracy less than 2'' ('' is basic unit of Angle), and the attitude output accuracy can be improved from 200'' to 10''.

Aiming at heavy workload, low efficiency, and slow running speed of manual diagnosis and recovery of soft faults of the inertial navigation system, [97] proposed a method of automatic diagnosis and recovery of soft faults based on the error model of the rotary inertial navigation system to quickly achieve the regular diagnosis and recovery of INS soft faults. [97] could realize stable and accurate navigation of INS. The Soft Fault Diagnosis Recovery (SFDR) method based on the RINS error model was used to find the fault

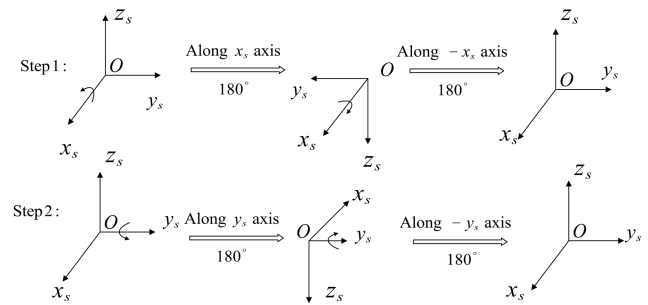


**FIGURE 7.** Calibration scheme for non-orthogonal angles in tri-axis RINS [89].

parameters by the least square method. After finding the fault parameters, a rotation strategy was designed. The recovery parameters were used to compensate for the outputs of three gyros and three accelerometers to recover soft fault parameters. According to the real biaxial RINS test, the SFDR method gradually found soft errors. It adopted an iterative algorithm with the advantages of fast fault identification, recovery, and high accuracy. The scale factor error of the gyro and accelerometer could achieve 6 ppm and 10 ppm accuracy, and the error of the gyro and accelerometer can reach 1'' and 2'' accuracy.

Aiming at principal model error and calculation error in the traditional-based in-motion attitude determination alignment (IMADA) alignment method, [98] proposed an improved Multistage IMADA (MIMADA) based on two-speed modeling. As demonstrated in Fig. 8, the traditional-based IMADA was used for first-level alignment to obtain the initial constant attitude matrix. This matrix can obtain the navigation-frame speed and then can be updated accurately. The model can realize the second-level alignment, and the initial strap-down matrix can be obtained after the alignment from 1 to then the strap-down INS (SINS) can be finely calibrated. Through 30 groups of simulation experiments, it is verified that this method is feasible. This method has certain positive significance in solving the design defects of traditional IMADA based on reducing the high-level alignment degradation of multi-level IMADA, weakening the relationship between alignment accuracy and vehicle speed, reducing the heading degradation times of secondary alignment from the original 20 times to 10 times, and improving the heading alignment accuracy by 23%.

Aiming at the problem that SINS/OD is difficult to obtain a high-precision attitude and position quickly and independently. Reference [99] proposed a motion alignment scheme based on backtracking, which can improve attitude accuracy quickly and independently and realize high-precision positioning. As demonstrated in Fig. 9, the method was divided into coarse and fine. The coarse alignment was defined as Improved Optimization-Based Coarse Alignment (IOBCA), which used the method proposed in [100] and the optimized attitude determination scheme. The attitude and position were obtained through known information



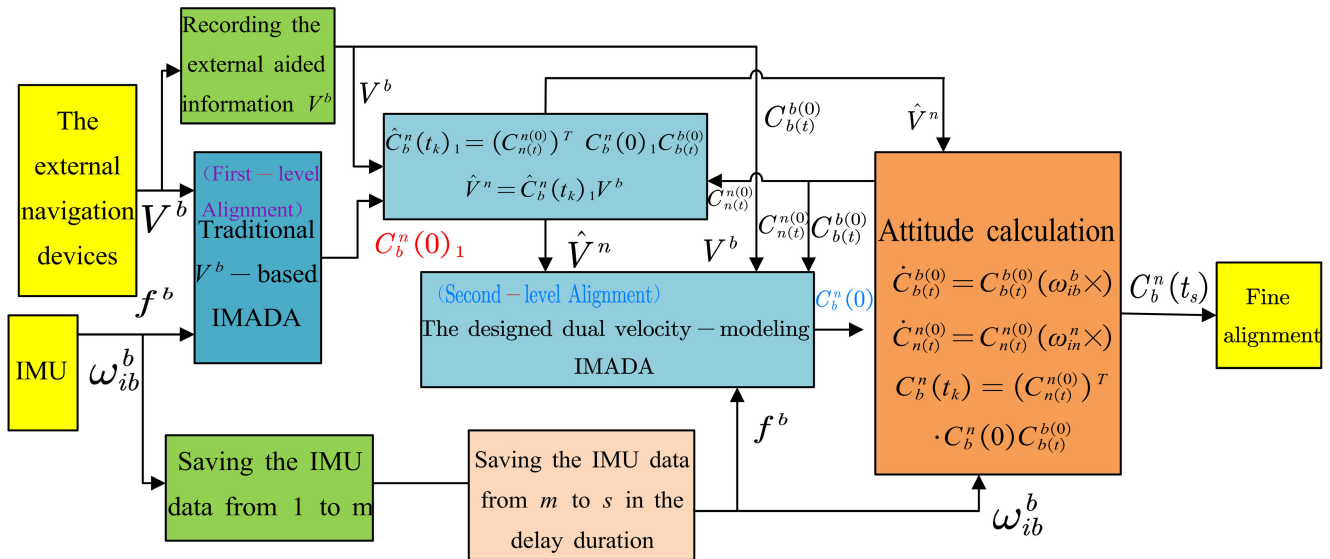


FIGURE 8. The block diagram of the improved multistage IMADA with the designed dual velocity-modeling IMADA [98].

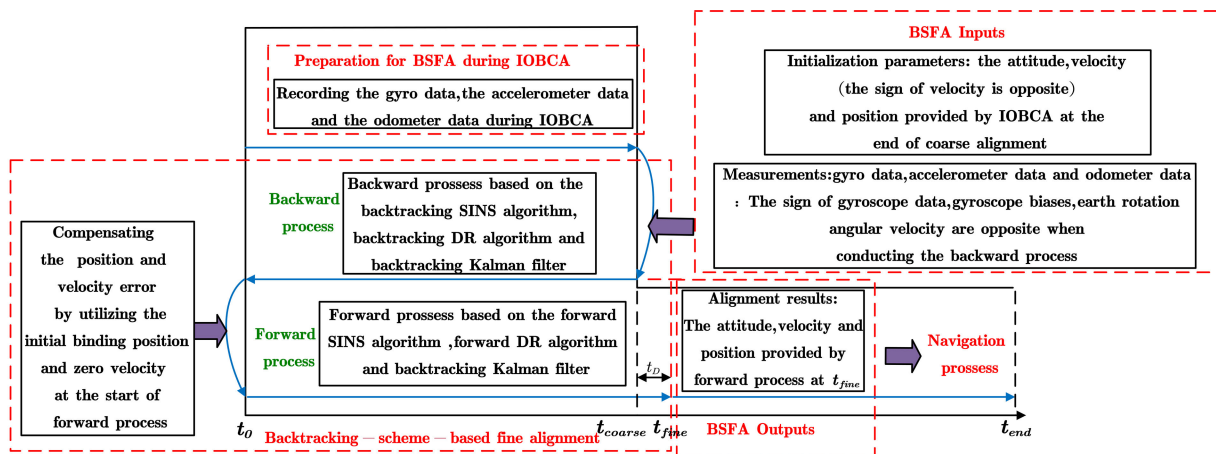


FIGURE 9. Diagram of the BSFA for OD-aided SINS [99].

such as initial binding position and zero speed. Then, according to the alignment result and initial information of IOBCA, through a Backtracking-Scheme-based Fine Alignment (BSFA) combined with the KF method, the known initial information was used to suppress the speed and position errors. It could optimize the attitude and improve the position accuracy. Three field tests demonstrate that this method could improve attitude accuracy quickly and obtain a high-precision position. It only applied to the navigation-level strap-down inertial navigation system combined with a high-precision outer diameter.

In light of the problem that the longer the lever arm of the SINS/OD and the faster the turning speed, the more significant the speed difference would be, which would lead to the lower precision of integrated navigation, [101] proposed an integrated navigation method based on coupled odometer and SINS. In this method, three Fiber-Optic

Gyroscopes (FOG) were used to measure the pitch angular velocity, roll angular velocity, and yaw angular velocity of the vehicle. Three accelerometers were used to measure the vehicle's forward, lateral, and vertical acceleration. After calculation, the primary navigation information is obtained, and the influence of the lever arm could be weakened by track estimation using two odometer speeds containing the lever arm information. As demonstrated in Fig. 10, the difference between the speed and position information of SINS/ODS was used as observation data to estimate the state vector of KF. The error estimates from the KF would be used to compensate for the primary navigation results (attitude, velocity, and position errors). Through navigation simulation, it is known that the integrated navigation method proposed in [101] is applied to a wide range of scenes. Its positioning accuracy was improved compared with the traditional integrated navigation method.

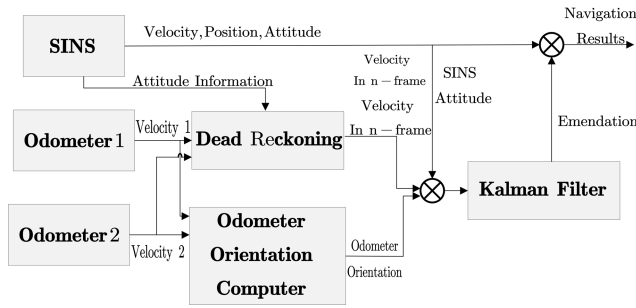


FIGURE 10. Schematic for the integrated navigation method [101].

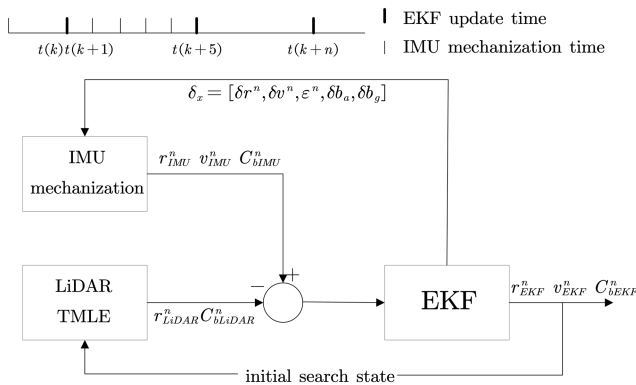


FIGURE 11. The system architecture of the LiDAR-aided inertial navigation system [102].

Aiming at the problem, the drift errors of velocity, position, and heading angles in INS will accumulate over time. The matching error of SLAM will also accumulate significantly in the featureless environment. Reference [102] proposed a Loosely Coupled EKF navigation system integrated with INS/ LiDAR SLAM. The system is demonstrated in Fig. 11. The model prediction state and measurement update state belong to the KF algorithm. The output frequency of LiDAR measurement is lower than IMU. The raw IMU output can narrow the search range of SLAM and improve search efficiency. The SLAM and IMU mechanization results are fused on the Loosely Coupled EKF navigation system. The results of various static and dynamic experiments demonstrate that IMU mechanization provides better attitude estimation in the dynamic test. The method proposed in [102] can still maintain centimeter-level accuracy in a featureless environment.

**IV. DIFFERENT ALGORITHMS FOR GNSS/INS INTEGRATED NAVIGATION**

In order to let the majority of scholars have a deeper understanding of the development of GNSS/INS integrated navigation and positioning technology for autonomous vehicles, this section screens out classic algorithms from algorithms summarized in this paper. As shown in Fig. 12, these algorithms are classified into four categories: Tightly Coupled GNSS/INS, Loosely Coupled GNSS/INS, Semi-tightly Coupled GNSS/INS, and Ultra-tightly Coupled

GNSS/INS, and all algorithms are described and analyzed in detail.

In this paper, we analyze and summarize each category’s typical GNSS/INS integrated navigation algorithms. Furthermore, these algorithms are compared from the following aspects:

- Sensitivity of capture: GNSS navigation and positioning function can be realized only when electromagnetic wave signals emitted by navigation satellites are obtained. And the acquisition sensitivity is the most crucial signal acquisition performance.
- Positioning accuracy: The positioning accuracy can reflect the positioning ability of integrated navigation. However, GNSS/INS combined navigation with different coupling modes has specific differences in positioning accuracy.
- Dynamic performance: GNSS/INS integrated navigation dynamic positioning accuracy when the receiver is in motion.
- Anti-interference: In the case of a low signal-to-noise ratio of satellite navigation signal or even signal interruption, the navigation solution can still be obtained.

Readers can refer to the classification method of GNSS/INS integrated navigation algorithms and the classification results of TABLE 2 in this paper. From sensitivity of capture, positioning accuracy, dynamic performance, and anti-interference to get algorithms divided into four coupling modes: ultra-tight coupling, deep coupling, loose coupling, and semi-tight coupling. The appropriate coupling mode is selected to solve the problem according to the actual needs.

**A. TIGHTLY COUPLED GNSS/INS**

Aiming that the performance of GNSS is degraded due to the NLOS reception, under the background that GNSS positioning technology is widely used in the location of urban canyons. Reference [21] proposed a close coupling integrated positioning method of 3D building model aided (3DMA) GNSS/INS, which could be divided into solution-based and grid-based methods. As demonstrated in Fig. 13, this system is divided into two integration methods. Red is a Loosely Coupled integration method, and blue is a Tightly Coupled integration method. Firstly, the 3DMA GNSS shadow matching positioning algorithm performs GNSS measurement through the initial position obtained by GNSS pseudo-range measurements and weighted least square positioning. Then, the solution-based method is to estimate the satellite’s position by matching the shadow with the surrounding building model to predict the visibility of the satellite. A grid-based method is used to indicate the visibility of satellites by using candidate positions’ visibility and score information during shadow-matching positioning. IMU is used to solve the inertial navigation equation by measuring the target’s linear acceleration and angular rate. Loosely Coupled method, the predicted satellite visibility can exclude GNSS NLOS measurements, and the least square method

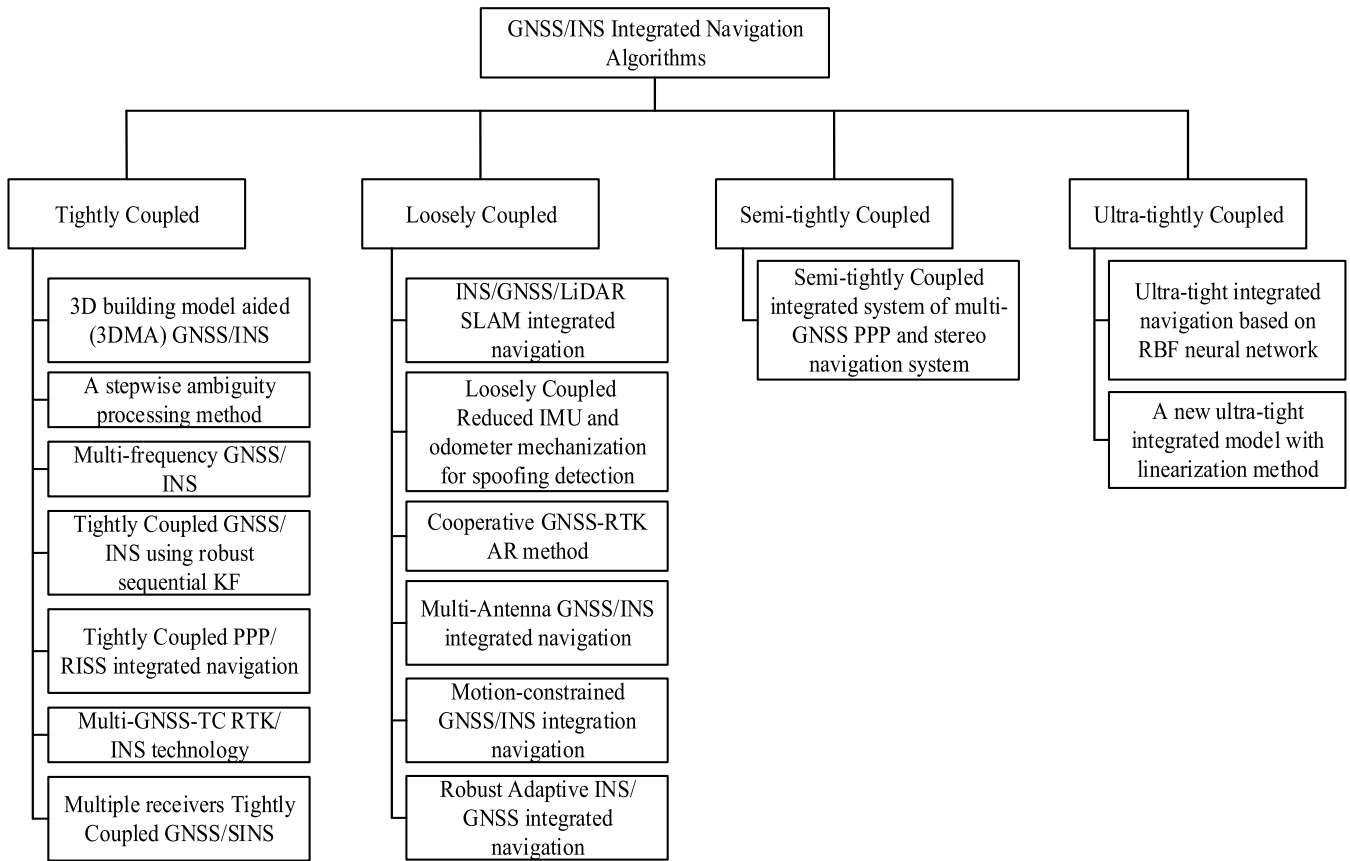


FIGURE 12. Classification of GNSS/INS integrated navigation algorithms.

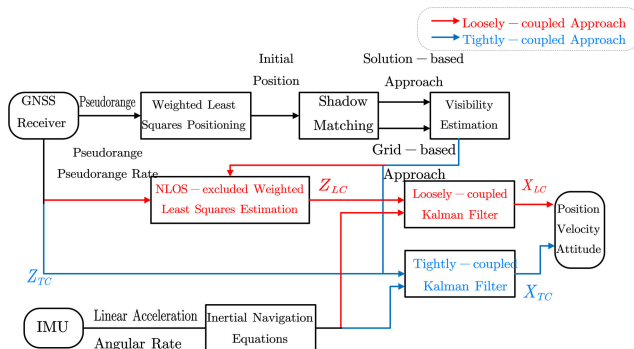


FIGURE 13. The flowchart of the proposed shadow matching aided the GNSS/INS integrated positioning system [21].

is applied to the GNSS measurements excluding NLOS to estimate the position and speed of the target. Combined with the results of INS, the final position, velocity, and attitude estimation can be obtained. In the Tightly Coupled method, the final result can be obtained by combining GNSS measurements with INS estimates using KF. The experimental results in different scenes, such as Light Urban, Middle Urban, Dense Urban, and Intersection, demonstrate that the proposed two satellite visibility estimation methods

have achieved more than 80%. Line-of-sight (LOS)/NLOS classification accuracy in most places in urban areas is at least 10% higher than the conventional method. Compared with the traditional GNSS/INS combination method, the precision of the proposed 3DMA GNSS/INS Tightly Coupled method is about 3 times higher.

To solve the problem of low navigation and positioning accuracy, discontinuity, and stability in open sky and GNSS signal occlusion environment, [59] proposed a TC GNSS/INS/OVS integrated navigation system based on fault detection and processing FDP method. As demonstrated in Fig. 14, the adaptive fault-tolerant integrated filter consists of three aspects: time update, fault detection and processing, and measurement update. Firstly, the time update is to realize the system state prediction and the corresponding error covariance update. Secondly, the FDP algorithm detects the fault and determines the fault treatment method. Finally, the measurement update equation should be calculated again with the adjusted measurement noise covariance matrix and measurement matrix due to the changing measurement noise covariance matrix and measurement matrix. Through the above steps, the integrated navigation system can obtain high-precision, continuous, and stable navigation results. The road test results demonstrate that the position

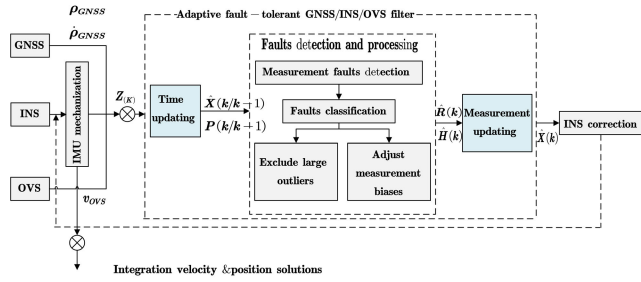


FIGURE 14. Adaptive fault-tolerant TC GNSS/INS/OVS integration navigation system architecture [59].

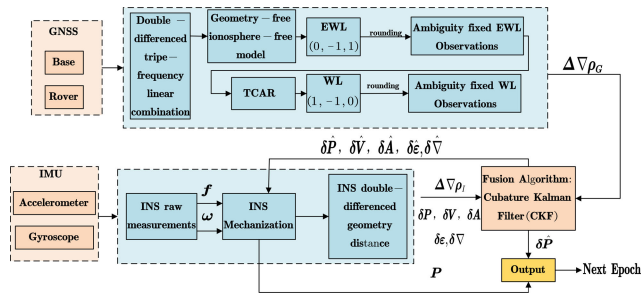


FIGURE 15. Integrated navigation structure diagram [63].

solution of the TC triple integrated system is more accurate than that of a Loosely Coupled (LC) integrated system. TC GNSS/INS/OVS integrated navigation system based on the FDP method can provide continuous and stable navigation and positioning and has good fault tolerance.

Aiming for poor stability and continuity of integrated positioning in GNSS/INS integrated navigation due to frequent signal occlusion, [63] proposed an improved Tightly Coupled algorithm. A stepwise ambiguity processing method is adopted to form instantaneous fixed Wide-Lane (WL) observations, which are used to correct inertial navigation measurement. Then, by estimating the differential inter-system bias (DISB) parameter, pivot satellites can be shared among different constellations, increasing the number of available satellites. As demonstrated in Fig. 15,  $p, f, \omega$  (the original measured value of the INS sensor) indicates the position, specific force, and angular velocity of the accelerometer and gyroscope. The experimental results of semi-simulated data sets demonstrate that the horizontal positioning accuracy reaches 4.1 cm and the vertical positioning accuracy reaches 15.2 cm when the satellite signal transmission is blocked. The proposed method in [63] achieves decimeter accuracy, which is significant to the high-precision positioning effect of GNSS/INS Tightly Coupled in a dense urban environment.

To solve insufficient research on multi-frequency and multi-system Tightly Coupled positioning methods in a dynamic urban environment, [67] was based on the GPS/BDS-2/INS three-frequency TC positioning model. Beidou-3 navigation satellite system four-frequency observation was introduced, and the performance of GPS/BDS-2/

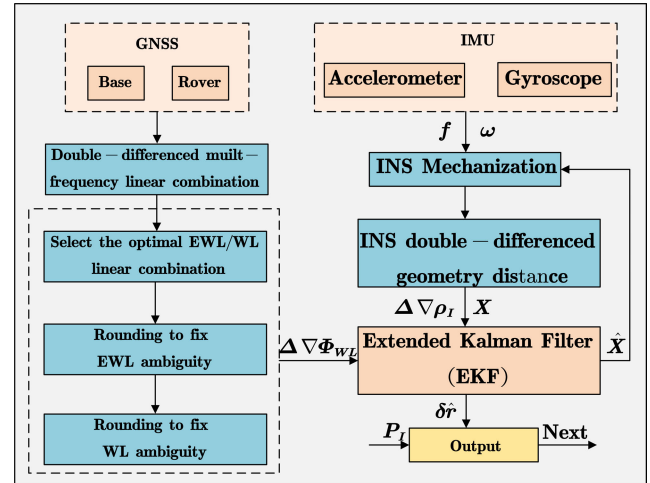


FIGURE 16. The flow chart of the multi-frequency GNSS/INS Tightly Coupled positioning method [67].

BDS-3/INS Tightly Coupled positioning was preliminarily studied. The process diagram of the multi-frequency and multi-system Tightly Coupled positioning algorithm is demonstrated in Fig. 16. The system can adapt the Beidou-3 four-frequency DD linear combination observation model, selecting the best extra-wide-lane/wide-lane (EWL/WL) remote sensing of the Beidou-3 four-frequency according to the regulations, adopting geometry-free (GF) model, applying triple-frequency carrier ambiguity resolution (TCAR) method to GPS/BDS-2 three-frequency observation and four-frequency carrier ambiguity resolution (FCAR) to BDS-3 four-frequency observation to solve the EWL/WL ambiguity problem. Finally, the EKF uses the difference between WL observation with fixed ambiguity and DD geometric distance calculated by INS and then corrects the approximate coordinates calculated by INS through estimation error to obtain the high-precision positioning result at the current moment. The experimental results demonstrate that the positioning accuracy of Tightly Coupled BDS-3/INS is higher than that of triple-frequency BDS-2/INS. Compared with GPS/BDS-2/BDS-3/INS, the positioning accuracy of Tightly Coupled GPS/BDS-2/BDS-3/INS in horizontal and vertical directions is improved by 29.1% and 58.7%, respectively.

Whether the parameters of IMU and receiver satisfy the dynamic loop requirement is the critical problem for Tightly Coupled, [103] proposed a new Tightly Coupled mathematical model, which analyzes the properties of error propagation through the principle of the norm. The stability of the tracking loop is judged by establishing an inequality containing most of the parameters of the Tightly Coupled navigation system. The Tightly Coupled algorithm proposed in [103] is demonstrated in Fig. 17. Doppler frequency and code phase deviation extracted from inertial information and satellite ephemeris are the keys of IMU-assisted Tightly Coupled. Mastering the critical information can control the

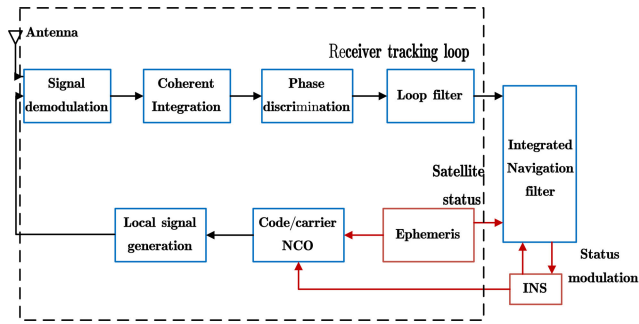


FIGURE 17. Structure diagram of the GNSS/INS deeply coupled system [103].

code/carrier Numerically Controlled Oscillator (NCO) in the tracking loop to ensure the high performance of the tracking loop under the condition of narrow bandwidth. The experimental results demonstrate that the method proposed in [103] is consistent with the simulation results, which verifies the correctness of this method.

Aiming at the accuracy, robustness, and computational efficiency of GNSS/INS integrated navigation, [104] proposed a Tightly Coupled GNSS/INS integrated algorithm using robust sequential KF. This method uses pseudo-range and Doppler and implements GNSS/INS data fusion by the time differenced carrier phase measurement. The KF measurement is performed sequentially, and a new robust estimation method detects and eliminates the signal fault. The frame diagram of the Tightly Coupled GNSS/INS integration algorithm is demonstrated in Fig. 18. In the figure, the solid line represents INS's high-rate information flow, and the dotted line represents GNSS's low-rate information flow. High-speed navigation results (position, attitude, speed) are calculated by INS mechanization through compensated raw INS data. The GNSS receiver provides low-rate pseudo-range, Doppler, carrier phase, and ephemeris data. Then systematic errors should be corrected by combining empirical models and different techniques. The updated GNSS observations and INS-predicted counterparts form the observed-minus-computed (OMC) measurements. The error is estimated by robust sequential KF using OMC measurements. The error state is returned to the INS to correct the navigation solution and INS sensor deviation. Field vehicle experiments demonstrate that the method proposed in [104] improves the accuracy of velocity and attitude by 69.42% and 47.16%, respectively, compared with Loosely Coupled. Compared with the traditional Tightly Coupled, it increased by 64.75% and 30.88%, respectively. Compared with batch KF processing, the computational efficiency is increased by 53.09%. This method can quickly complete the bridging work in the case of partial or complete interruption of GNSS.

Because GNSS signals are more likely to be blocked and interrupted, which affects the accuracy of navigation and positioning, PPP/INS integrated navigation can reduce the influence of GNSS. However, due to the high price of

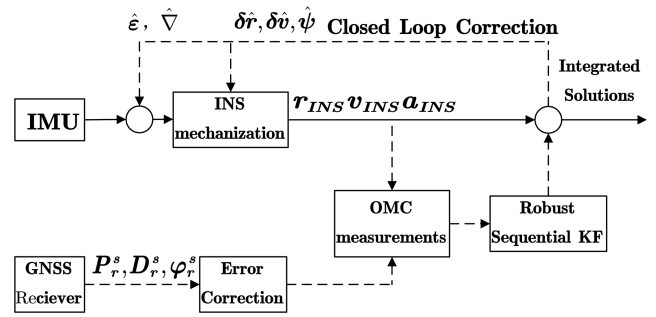


FIGURE 18. GNSS/INS integration through a robust sequential KF [104].

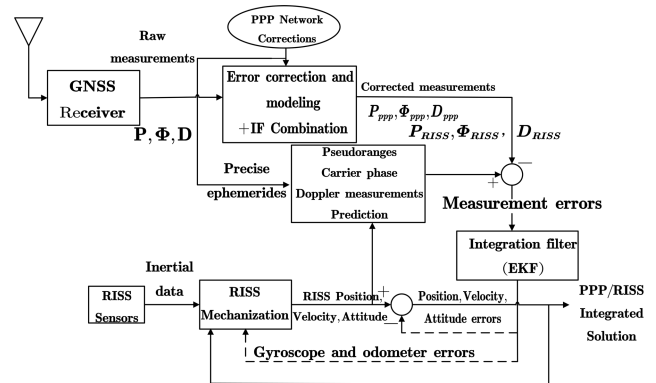


FIGURE 19. Block diagram of the developed TC PPP/RISS integrated system [38].

high-end INS, it may not be widely used in automobiles. To solve this problem, [38] proposed combining INS and RISS to achieve lane-level car navigation. The frame diagram of PPP/RISS integrated navigation is demonstrated in Fig. 19. The GNSS receiver acquires the raw pseudo-range, carrier phase, and Doppler measurements. The PPP network correction and error model corrects this information. Meanwhile, RISS mechanically outputs the measured value. EKF takes the difference between the predicted and actual GNSS measurements as measurement errors. The measurement errors will be fed to an EKF. The estimated position, velocity, and attitude are obtained by filtering the measurement error and the corresponding error operation of the system error model. The estimated values of navigation parameters will be fed back to the RISS mechanization module. The estimated error of the sensor can correct the deviation of the sensor. In the feedback process, the error state of each epoch is reset to keep the linearity assumption of EKF. The road test experiment demonstrates that the root mean square error of the PPP/RISS integrated system can be maintained at a level of less than 20 cm, and the maximum error is less than 50 cm. Compared with PPP alone, PPP/RISS integration can provide a continuous and stable solution, and the re-convergence time after GNSS interruption is shorter.

Accurate ambiguity estimation of Tightly Coupled GNSS/INS is critical to accurate navigation and positioning. Aiming at the ambiguity estimation problem in Tightly

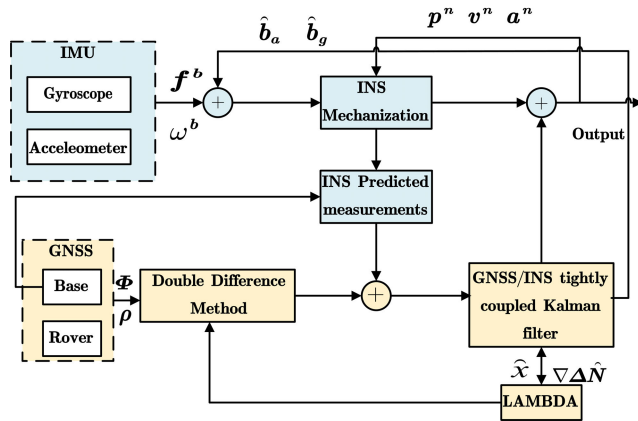


FIGURE 20. The principle of GNSS/INS Tightly Coupled ambiguity resolution [105].

Coupled GNSS/INS, [105] proposed a new ambiguity estimation and elimination strategy. The schematic diagram of Tightly Coupled GNSS/INS ambiguity resolution is demonstrated in Fig. 20. In this scheme, the ambiguity parameter of the carrier phase is added to the state equation of the filter for estimation. The observation model of single-frequency and the wide-lane combination is used to assist in ambiguity fixed. By using the method of parameter elimination, when the ambiguity parameters are fixed without cycle slip, the ambiguity parameters are removed from the state equation to reduce the computational complexity. The residual test method is adopted. After each epoch is estimated, the estimation deviation and outliers need to be tested by residual test to avoid the influence of satellite ambiguity estimation deviation on the next epoch. Through the experiment, the results demonstrate that in the open sky environment, the positioning error of Tightly Coupled GNSS/INS proposed in [105] is less than 5 cm, and the ambiguity fixed rate is more than 97%, which is consistent with the GNSS positioning results. Without GNSS, the positioning accuracy of GNSS/INS is better than that of GNSS, and the positioning accuracy in X, Y, and Z directions is improved by 82.46%, 78.87%, and 79.67%, respectively. The fixed rate of ambiguity increased from 73% to 78.57%. Overall, the Tightly Coupled GNSS/INS proposed in [105] has a higher ambiguity fixed rate. The navigation and positioning results are stable, continuous, and accurate.

Seamless positioning technology in a complex environment is a research hotspot of autonomous vehicles (AVs). Because of the multipath effect, an insufficient number of satellites, easy interruption of GNSS signals, and poor quality of indoor GNSS signals, the integration of multi-GNSS and INS cannot provide good seamless positioning results for indoor and outdoor AVs. To solve this problem, [106] developed a multi-GNSS-TC RTK/INS technology. Ultra-Wideband (UWB)/INS technology provides continuous and accurate navigation and positioning results for indoor environments. An improved adaptive robust extended Kalman filter (AREKF) algorithm based on TC integrated single

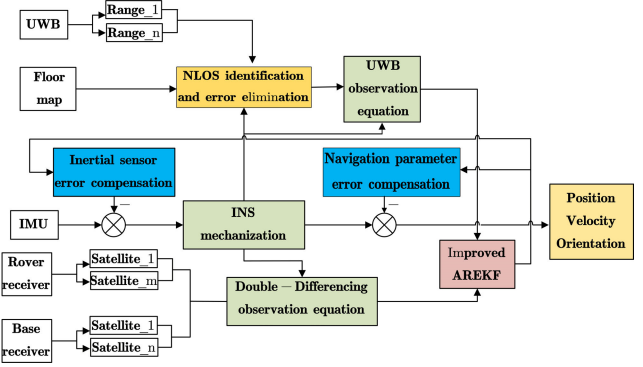


FIGURE 21. Algorithm flowchart [106].

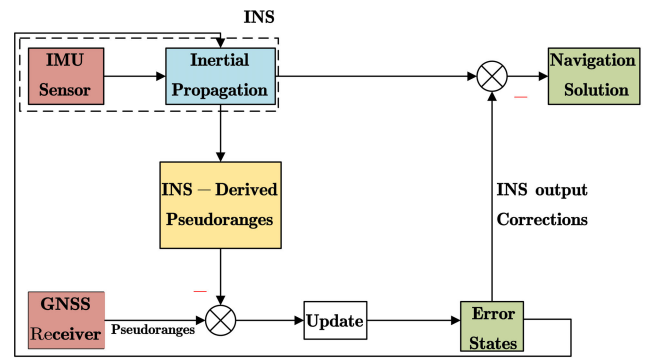


FIGURE 22. Closed-loop error-state GNSS/INS tight integration architecture [107].

frequency multi-GNSS-TC RTK/UWB/INS map system is studied to provide continuous, reliable, and high-precision navigation information for indoor and outdoor AVs. In TC integrated system, carrier phase observations, and GNSS code will be affected by multipath errors, and the accuracy of code observation and UWB ranging will also be affected by multipath propagation. The accuracy of GNSS floating-point solutions will be affected by the observation errors. The improved AREKF algorithm is used to adjust the variance of outliers. The flow chart of the algorithm is demonstrated in Fig. 21. The experimental results demonstrate that the RMS accuracy of the algorithm and the system in the north, east, and two-dimensional directions are 0.1756 m, 0.1698 m, and 0.2443 m, respectively. The average errors in the north, east, and two-dimensional directions are 0.0932 m, 0.1049 m, and 0.1657 m, respectively. The maximum errors in the north, east, and two-dimensional directions are 0.7986 m, 1.0632 m, and 1.1372 m, respectively. This scheme has high positioning accuracy and stability in indoor, transitional, or outdoor environments.

Aiming at the undetected or IMU fault of Tightly Coupled GNSS/INS integration, [107] proposed an effective fault detection and exclusion scheme. The integrated model is demonstrated in Fig. 22. It is derived to capture GNSS faults and filter faults. The EKF error in the integrated model will be fed back during iteration to correct the system,

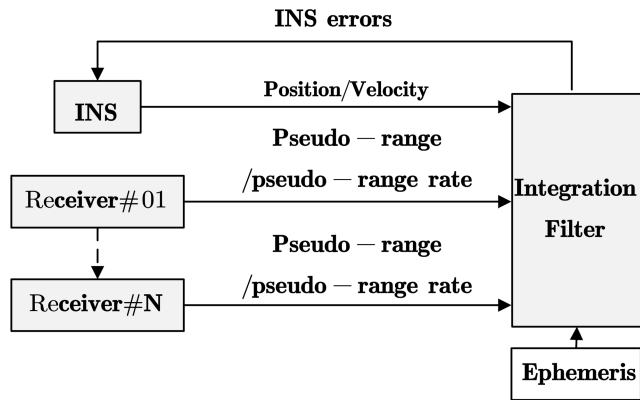


FIGURE 23. Basic structure of multiple receivers based GNSS/SINS tight integration system [108].

maintaining a linear approximation of the system model. GNSS measurement is an external aiding of Tightly Coupled GNSS/INS, which is used to correct INS solutions and compensate for inertial sensor errors. It is assumed that two independent detectors are used to detect GNSS and filter faults, and then the system will recover independently to eliminate the influence of filter faults. The simulation experiment proves that the scheme can always maintain high efficiency and effectiveness when a fault occurs.

GNSS can obtain accurate navigation results by observing a sufficient number of satellites, but when the signal quality decreases, the positioning capability of GNSS will be affected. However, INS contains random noise, so the positioning error accumulates with time. To solve this problem, [108] proposed multiple receivers Tightly Coupled GNSS/SINS scheme, adopting the measurement difference method to improve the calculation efficiency. The frame diagram of GNSS/SINS based on multiple receivers is demonstrated in Fig. 23. The integration filter’s measurement vector consists of multiple receivers’ pseudo-range and pseudo-range rates. Measurement differences can reduce the dimension of the state vector. The integration filter estimates the INS error, feeds it back, and compensates the INS. The compensated INS navigation solution is outputted as a result. The experiment demonstrates that the navigation and positioning accuracy of the Tightly Coupled multi-receiver GNSS/INS proposed in [108] is higher than that of the Tightly Coupled single-receiver GNSS/INS. The feasibility of the measurement difference method can be verified.

**B. LOOSELY COUPLED GNSS/INS**

Aiming at low positioning accuracy and poor navigation effect due to weak GNSS signals in actual navigation and positioning, [62] proposed an INS/GNSS/LiDAR SLAM integrated navigation system. This system makes up for the deficiency of the integrated system by acquiring all the information received by each sensor. The integrated navigation system is demonstrated in Fig. 24. The refreshed grid-based SLAM and updated mechanization (red and green

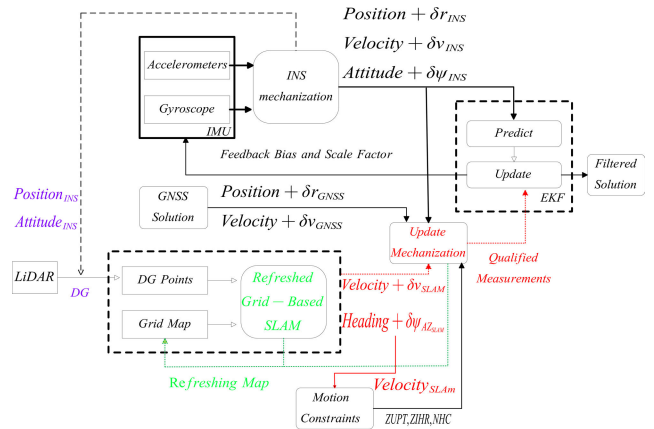


FIGURE 24. Data processing of INS/GNSS/Refreshed-SLAM fusion algorithm [62].

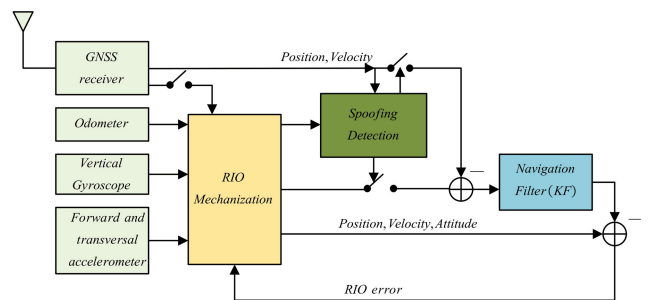


FIGURE 25. Loosely Coupled RIO mechanization for spoofing detection [66].

marks in the figure) are adopted in the system, which enriches and expands the traditional GNSS/INS integrated navigation. The refreshed grid-based SLAM (blue mark in the figure) obtains the initial value from Direct georeferencing (DG). At the same time, GNSS/INS needs the support of the refreshed grid-based SLAM. The updated mechanization authenticates all the measured values of the system. The experimental results demonstrate that, compared with the traditional GNSS/INS integrated navigation system, this system provides absolute navigation accuracy of 2 meters and 0.6% of distance traveled when the GNSS signal is interrupted. In the case of a weak GNSS signal, the navigation accuracy reaches 1.2 meters.

Aiming at the phenomenon that GNSS signal spoofing threatens the security and privacy of unmanned driving, [66] proposed a spoofing detection method based on a consistency check between GNSS and IMU/odometer mechanization. The method analyzes the measurements of GNSS and IMU/odometer independently and checks the mechanization solutions of GNSS and INS/odometer, respectively. The mechanized frame diagram of Loosely Coupled Reduced IMU and odometer (RIO) for deception detection is demonstrated in Fig. 25. RIO can provide relative position, velocity, and heading information by mechanically receiving forward velocity information, raw accelerometer, and gyroscope measurements. During the observation interval, the authenticity

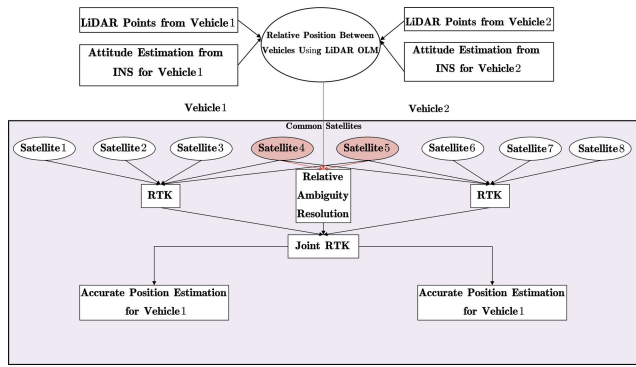
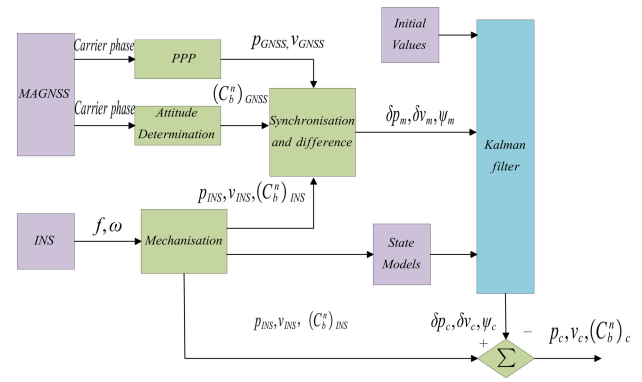


FIGURE 26. Flowchart of methods [109].

verification unit will compare GNSS’s navigation solution with RIO. If the solution is feasible, the GNSS solution corrects the RIO solution, and the navigation KF corrects the accelerometer and gyroscope. Finally, the actual vehicle experiment verifies the feasibility of the method proposed in [66]. The spoofing detection performance of the method in sub-urban and dense urban environments is evaluated.

Aiming at the problem of low satellite visibility of single vehicles, the ambiguity resolution (AR) is easy to fail in the urban occlusion environment. To solve this problem, [109] proposed a cooperative GNSS-RTK AR method. Use navigation data of multiconnected vehicles to improve AR. Improve GNSS, RTK, and AR through centralized processing of multiconnected vehicles’ GNSS, INS, and LiDAR data. High-precision positioning results can be obtained by the map-matching algorithm of the occupancy likelihood map (OLM), which connects the relative positions between vehicles. The flowchart of the method is demonstrated in Fig. 26. A joint RTK algorithm is proposed to enhance AR performance by fusing the observation data of all connected vehicles. The relative position between vehicles establishes the position constraint between vehicles. Constraints can be calculated by the LiDAR OLM method and attitude information of INS. Finally, the final position estimations of connected vehicles with relative position and ambiguity constraints need the information of joint RTK. The experimental results demonstrate that compared with the standard RTK AR method for a single vehicle, the performance of RTK AR is improved in terms of ratio values, success rate, and fixed rate by the method proposed in [109]. The vehicle positioning accuracy is also improved. Even if the GNSS signal is blocked, the ideal navigation and positioning results can still be obtained.

Since the position accuracy of PPP/INS is comparable to that of DGNSS/INS. Still, the poor yaw angle accuracy leads to low positioning accuracy under dynamic conditions, [24] proposed a Multi-Antenna GNSS (MAGNSS)/INS integrated navigation system. The flow chart of this integrated navigation is demonstrated in Fig. 27. Because of the errors of gyros and accelerometers, INS mechanized navigation solutions may drift, and the precision of gyros and accelerometers



$b$ : body frame  $n$ : navigation frame

$f$ : specific force  $\omega$ : angular rate  $p$ : position  $v$ : velocity  $C$ : attitude matrix

subscript  $m$ : measurements subscript  $e$ : estimation  $\delta$ : error

FIGURE 27. Flow chart of MAGNSS/INS integrated navigation [24].

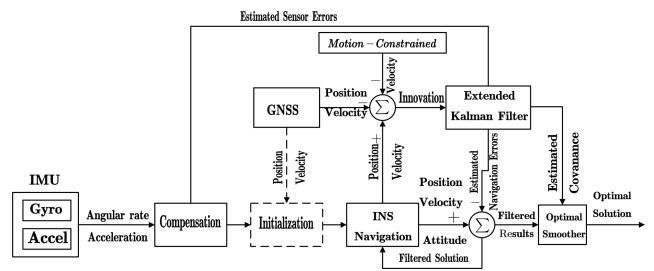
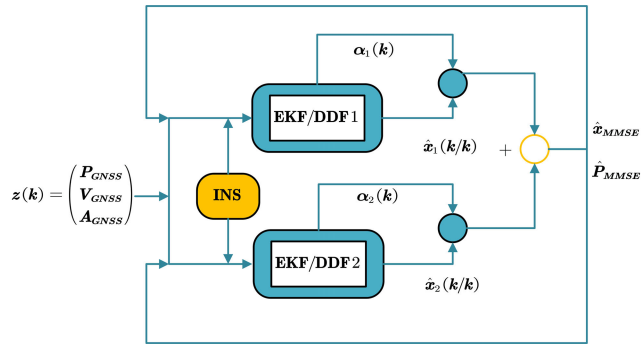


FIGURE 28. Flowchart of motion-constrained GNSS/INS integration for the track irregularity measurement [29].

determines the drift rate. The external system can estimate the navigation error to realize a stable navigation scheme. The differential equations of the misalignment angle, velocity error, and position error are the error equation of INS. The experimental results demonstrate that the position, roll, and pitch accuracy of the PPP/INS integrated navigation system are higher. Still, the accuracy of yaw is lower when tactical-grade INS is adopted. The MAGNSS/INS proposed in [24] solves the problem of low yaw accuracy of PPP/INS. MAGNSS/INS integration realizes low-cost and high-precision positioning without a base station.

Because of the low spatial accuracy of GNSS/INS integration applied to track geometry measurement, the relative spatial accuracy threshold values satisfying the constraint of shortwave track irregularity measurements are derived in [29], and the GNSS/INS integration is constrained. The flow chart of the integrated system is demonstrated in Fig. 28. Error compensation means that the output of inertial sensors is corrected by sensor error and then input into the navigation algorithm. The estimated sensor errors of optimal estimation can adjust the corresponding raw IMU measurements. The dotted line part in the figure is navigation initialization, which provides initial attitude from different alignment methods to maintain high-precision initial navigation. Generally, the GNSS or input manually provides the initial position and velocity. Mechanization is to update





**FIGURE 29. Robust Adaptive INS/GNSS integrated navigation system [110].**

the velocity and position of INS by rotating and integrating the acceleration measurement, and the attitude of INS is calculated by compensating the gyroscope measurements. The EKF will update the measurements according to the position and velocity information provided by the navigation system. The influence of INS drift error is reduced by the optimal smoother to achieve the high-precision post-processing application. The field test demonstrates that the accuracy of GNSS/INS integration with motion constraints is relatively high, and the accuracy requirements of shortwave track vertical irregularities can be met.

Aiming at the problem of state space model with non-Gaussian measurement noise, [110] proposed a robust GNSS/INS navigation system design based on parallel nonlinear filtering. Nonlinear approximation techniques such as EKF and Sigma Point Kalman Filter (SPKF) are adopted. A robust navigation system is designed, and the navigation state vector is estimated. The frame diagram of an integrated navigation system using robust adaptive GNSS/INS is demonstrated in Fig. 29. The simulation experiment demonstrates that the parallel architecture improves the efficiency during the rapid movement of the aircraft, and the non-Gaussian GNSS noise has affected the nonlinear filter slightly. The estimation results of parallel architecture and impulsive measurement noise environment are better than those of nonlinear filters such as EKF, UKF, and Central Difference Kalman Filters (CDKF).

### C. SEMI-TIGHTLY COUPLED GNSS/INS

Because of that Visual-Inertial Navigation Systems (VINS)/GNSS integrated navigation relies on the global position to eliminate the accumulated error, and the positioning level is not high, [61] proposed a Semi-tightly Coupled integrated system of multi-GNSS PPP and S-VINS. The algorithm implementation principle of the system is demonstrated in Fig. 30. The system must complete the visual-inertial initialization, apply the sliding window-based nonlinear optimization to the system state, and transform the local state into the global state in real-time by converting the local and global frames. The transformation matrix is initialized to the identity matrix and updated after global optimization. PPP data processing adopts the intermediate frequency (IF)

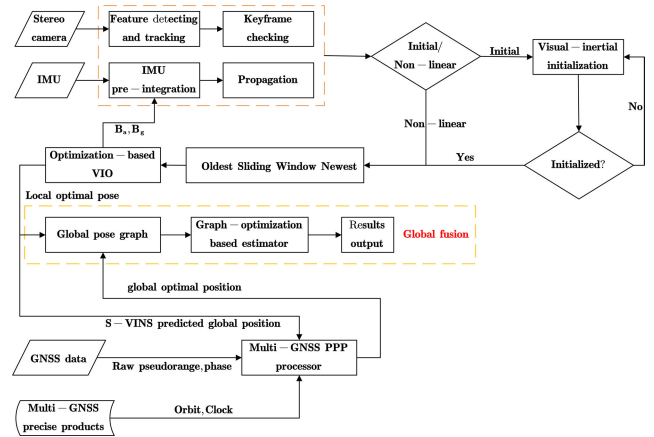


**FIGURE 30. Implementation of the graph-optimization-based semi-tightly Coupled framework of multi-GNSS PPP/S-VINS [61].**

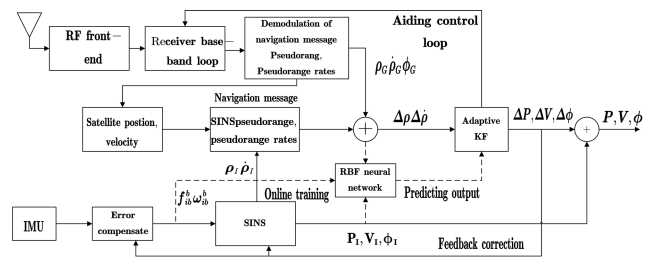


**FIGURE 31. Structure of ultra-tightly integrated navigation system based on RBF neural network [111].**

combination of GNSS raw pseudo-range and phase measurements. When the feedback mechanism is running, the predicted position of S-VINS is used for PPP data processing. Then the global fusion processor receives the global position and its uncertainty. After global optimization, the optimal positioning result is obtained. Finally, the conversion from the local to global frames is updated. The vehicle experiment results demonstrate that the multi-GNSS PPP/S-VINS Semi-tightly Coupled system will be 41.8-60.6% higher than the multi-GNSS PPP/INS system in terms of 3D positioning accuracy.

### D. ULTRA-TIGHTLY COUPLED GNSS/INS

To obtain navigation results that meet the accuracy requirements even when GNSS signals are weak, [111] proposed an ultra-tightly integrated navigation algorithm based on neural network-aided filtering, and a deeply integrated navigation system based on radial basis function neural network method is designed. The architecture of the integrated navigation is demonstrated in Fig. 31, which is divided into two stages. In the first stage, when the GNSS signal is good, the KF and neural network model are combined to control the error caused by the uncertainty of the model. In the second stage, when the GNSS signal is lock-losing, the neural network model of the first stage is used to predict the out-of-lock system model to curb the accumulated error of the inertial navigation system with time. Then, adaptive

KF is applied to the system state vector, and the estimated value is used to correct the error of INS. The experimental results demonstrate that the algorithm proposed in [111] can realize high-precision positioning and continuous and stable navigation of integrated navigation under weak GNSS signals, which verifies the practicability of the algorithm.

Aiming at the integrated structure system based on coherent cumulative measurements in-phase/quadrature ( $I/Q$ ) in GNSS/INS ultra tight integrated navigation has complexity and nonlinearity when  $I/Q$  is converted into navigation information, [64] proposed a new model and linearization method to be applied to the integrity, stability and hidden nonlinear factors of the system. A code phase approximation way without introducing new measurements is used for the positioning error caused by neglecting code-loop deviation. The Ultra tight integration system is demonstrated in Fig. 32. In this structure, the  $I/Q$  signal of the receiver is estimated by the information provided by INS, and the difference between the measured and estimated  $I/Q$  values of the receiver is taken as the observed value. The modified positioning information and ephemeris calculate the loop control parameters. Then, forming a vector tracking carrier loop. Reference [64] proposed an ultra-tight integration with code errors without re-measurement, as demonstrated in Fig. 33. This integrated system does not introduce early and late measurement and uses position error to approximate code delay and self-correlation function, coupled with  $I/Q$  prediction. It does not use a traditional scalar code-tracking loop, and its discriminator using and can be canceled. The experimental results of semi-physical simulation demonstrate that the new coding phase approximation method proposed in [64] greatly reduces the coding error rate during cyclic oscillation. It has high target positioning, speed, and attitude accuracy.

## V. SUMMARIES AND OUTLOOK

### A. SUMMARIES

In this paper, GNSS/INS integrated navigation algorithms are comprehensively summarized. As can be seen from TABLE-2, each algorithm has its characteristics:

In the GNSS/INS integrated navigation algorithms, except for the Ultra-tightly Coupled mode, the other integrated modes are challenging to capture GNSS signals quickly.

For different integrated modes in integrated navigation, the position accuracy of LC (see [62], [66], [110], [109], [24], [29]) is the lowest. The positioning accuracy of Tightly Coupled (see [21], [59], [63], [67], [103], [104], [38], [105], [106], [107], [108]) and Semi-tightly Coupled (see [61]) decreases in turn. Because the Ultra-tightly Coupling mode (see [111], [64]) has the strongest ability to estimate and correct the errors of INS. Thus, its positioning accuracy is the highest. Therefore, GNSS/INS integrated navigation with different coupling modes will affect autonomous vehicle navigation and positioning capabilities and safety.

In integrated navigation, both loosely coupled and Tightly Coupled use the output information of the GNSS receiver to

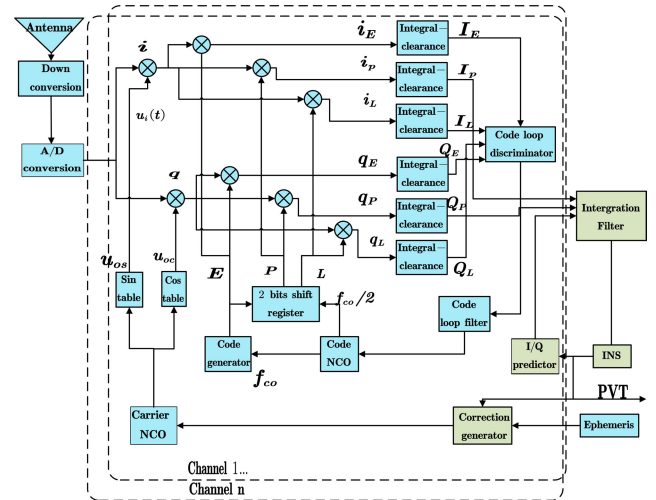


FIGURE 32. Ultra-tight integration considering code errors [64].

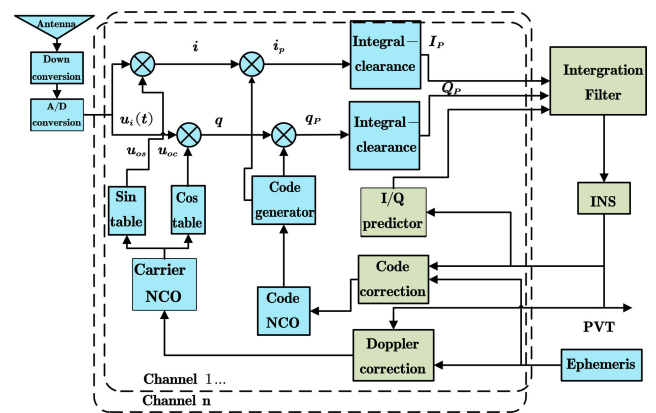


FIGURE 33. Ultra-tight integration considering code errors without new measurements [64].

assist INS, and the GNSS receiver is always independent. Thus, the anti-interference ability and dynamic tracking ability of these two modes still need to be enhanced. However, the Ultra-tightly Coupled cancels the carrier tracking loop. It directly uses the  $I/Q$  signal output by the correlator of the GNSS receiver as the input of the integrated navigation KF, realizing the mutual independence of measurement noise. Thus, the dynamic performance and anti-interference ability of the Ultra-tightly Coupled are the best.

Among the GNSS/INS integrated navigation algorithms selected in this paper, [66], [62], [109], and [59] are not simply combining GNSS and INS. Reference [59] is GNSS/INS/OVS integrated navigation. Reference [62] is INS/GNSS/LiDAR SLAM integrated navigation. Reference [66] is a spoofing detection method based on a consistency check between GNSS and IMU/OD mechanization. The GNSS, INS, and LiDAR data are applied in [109]. They both combine other sensors. This demonstrates that integrated navigation is developing from GNSS/INS to GNSS/INS combined with multi-sensors.

**TABLE 2. Comparison of GNSS/INS integrated navigation algorithms.**

	Algorithms	Sensitivity of capture	Positioning accuracy	Dynamic performance	Anti-interference	Only GNSS/INS sensors
Ultra-tightly Coupled	[111]	Good	Better	Better	Better	Yes
	[64]	Good	Better	Better	Better	Yes
Tightly Coupled	[21]	Average	Good	Good	Good	Yes
	[59]	Average	Good	Good	Good	No
	[63]	Average	Good	Good	Good	Yes
	[67]	Average	Good	Good	Good	Yes
	[103]	Average	Good	Good	Good	Yes
	[104]	Average	Good	Good	Good	Yes
	[38]	Average	Good	Good	Good	Yes
	[105]	Average	Good	Good	Good	Yes
	[106]	Average	Good	Good	Good	Yes
	[107]	Average	Good	Good	Good	Yes
[108]	Average	Good	Good	Good	Yes	
Semi-tightly Coupled	[61]	Average	Unknown	Good	Good	Yes
Loosely Coupled	[62]	Average	Average	Bad	Bad	No
	[66]	Average	Average	Bad	Bad	No
	[110]	Average	Average	Bad	Bad	Yes
	[109]	Average	Average	Bad	Bad	No
	[24]	Average	Average	Bad	Bad	Yes
	[29]	Average	Average	Bad	Bad	Yes

Overall, the Ultra-tightly Coupled is the best in capture sensitivity, positioning accuracy, dynamic performance, and anti-interference ability. The overall performance of Tightly Coupled and Semi-tightly Coupled deteriorate gradually. However, the capture sensitivity and positioning accuracy

of Loosely Coupled is average. Its dynamic tracking ability and anti-interference ability are the worst. Therefore, when the GNSS signal is partially blocked, the navigation and positioning accuracy of Ultra-tightly Coupled, Tightly Coupled, Semi-tightly Coupled, and Loosely Coupled decreases

in turn. However, considering the actual cost and different application requirements, these integrated modes have advantages and disadvantages.

Reference [112] is a review of the specific application of GNSS in bridge structural health monitoring. The application of GNSS can predict bridge faults in advance and efficiently, which is of great significance. Reference [113] is a review of the specific application of GNSS in railway signals in Europe. GNSS is an essential part of the European Train Control System (ETCS) as a low-cost signal solution for ETCS. Compared with [112] and [113], the novelty of our paper is as follows:

In addition to the application of GNSS, INS is also included in the survey of our paper, which is about the specific application of GNSS/INS integrated navigation algorithm in high-precision navigation and positioning.

Compared with bridge structural health monitoring of [112] and Train location information acquisition of [113], applying GNSS/INS integrated navigation algorithm in high-precision navigation and positioning is more challenging due to the increasingly complex vehicle driving environment. Therefore, the review of the application of GNSS/INS integrated navigation in autonomous driving navigation and positioning technology is of specific significance.

At present, the application of GNSS in bridge structural health monitoring and Train location information acquisition is developing slowly. With the rapid development of autonomous vehicles, GNSS/INS integrated navigation has sufficient development space in the aspect of high-precision navigation and positioning of driverless vehicles. Therefore, our paper accords with the development direction of GNSS and INS.

## B. OUTLOOK

Many innovative GNSS/INS integrated navigation algorithms have been developed to solve autonomous vehicles' navigation and positioning problems in recent years. However, the application of the GNSS/INS integrated navigation algorithm to automatic driving is still in the developing stage. In future research, it is still necessary to solve the problems of GNSS/INS integrated navigation systems, strikingly achieving high-precision navigation and positioning of self-driving cars. In this paper, the possible research hotspots of GNSS/INS integrated navigation are as follows:

Observation accuracy can affect the fixed performance of ambiguity in the dynamic positioning of GNSS, so it is necessary to research the stepwise ambiguity fixing method.

The filtering algorithm of GNSS/INS integrated navigation converges to the ideal accuracy costing a more extended period. Besides, the navigation and positioning results of the integrated navigation will be affected by the unlocked GNSS signal. To solve these problems, the research of a smoothing algorithm can significantly improve the parameter estimation accuracy of the filtering algorithm.

In the practical work of the GNSS/INS integrated navigation system, data loss caused by the failure of hardware

equipment often happens. Because of this situation, it is crucial to establish a prediction model for missing data and improve the accuracy of filtering results.

In the dynamic environment of automobile driving, the external environment will affect the accuracy of GNSS observations and the ambiguity-fixing performance. To solve this problem, INS can assist GNSS in fixing ambiguity. It can enhance the intensity of ambiguity variance and improve the precision of ambiguity floating point solution.

In GNSS/INS integrated navigation, different information fusion algorithms will be used to fuse GNSS and INS information. Thus, the navigation and positioning effects will be different. For example, the Ultra-tightly Coupled scheme, the accuracy of a dynamic model building of an integrated navigation system, and the statistical characteristics of system noise directly determine the accuracy and stability of KF in system state estimation. Therefore, a better robustness integrated navigation information fusion algorithm is needed for navigation and positioning.

## REFERENCES

- [1] T.-S. Lou, N.-H. Chen, Z.-W. Chen, and X.-L. Wang, "Robust partially strong tracking extended Kalman filtering for INS/GNSS integrated navigation," *IEEE Access*, vol. 7, pp. 151230–151238, 2019.
- [2] S. Lu, Y. Guo, H. Shang, K. Tang, J. Cao, R. Yu, and S. Cai, "Spoofing control strategy for precise position offset based on INS/GNSS tightly coupled navigation," *IEEE Access*, vol. 8, pp. 103585–103600, 2020.
- [3] W. Wen, X. Bai, G. Zhang, S. Chen, F. Yuan, and L.-T. Hsu, "Multi-agent collaborative GNSS/camera/INS integration aided by inter-ranging for vehicular navigation in urban areas," *IEEE Access*, vol. 8, pp. 124323–124338, 2020.
- [4] A. Yoganandhan, S. D. Subhash, J. Hebison Jothi, and V. Mohanavel, "Fundamentals and development of self-driving cars," *Mater. Today, Proc.*, vol. 33, pp. 3303–3310, Jan. 2020.
- [5] A. Abosekeen, U. Iqbal, A. Noureldin, and M. J. Korenberg, "A novel multi-level integrated navigation system for challenging GNSS environments," *IEEE Trans. Intell. Transp. Syst.*, vol. 22, no. 8, pp. 4838–4852, Aug. 2021.
- [6] M. Maaref and Z. M. Kassas, "Ground vehicle navigation in GNSS-challenged environments using signals of opportunity and a closed-loop map-matching approach," *IEEE Trans. Intell. Transp. Syst.*, vol. 21, no. 7, pp. 2723–2738, Jul. 2020.
- [7] Y. Zhang, L. Wang, X. Jiang, Y. Zeng, and Y. Dai, "An efficient LiDAR-based localization method for self-driving cars in dynamic environments," *Robotica*, vol. 40, no. 1, pp. 38–55, Jan. 2022.
- [8] J. M. Hansen, T. A. Johansen, N. Sokolova, and T. I. Fossen, "Nonlinear observer for tightly coupled integrated inertial navigation aided by RTK-GNSS measurements," *IEEE Trans. Control Syst. Technol.*, vol. 27, no. 3, pp. 1084–1099, May 2019.
- [9] J. Skorepa, P. Kovar, and P. Puricer, "PDOP parameters improvement using multi-GNSS and signal re-transmission at lunar distances," *Adv. Space Res.*, vol. 68, no. 9, pp. 3700–3716, Nov. 2021.
- [10] T. Szot, C. Specht, P. S. Dabrowski, and M. Specht, "Comparative analysis of positioning accuracy of garmin forerunner wearable GNSS receivers in dynamic testing," *Measurement*, vol. 183, Oct. 2021, Art. no. 109846.
- [11] W. Fu, Y. Yang, Q. Zhang, and G. Huang, "Real-time estimation of BDS/GPS high-rate satellite clock offsets using sequential least squares," *Adv. Space Res.*, vol. 62, no. 2, pp. 477–487, Jul. 2018.
- [12] Y. Guo, M. Wu, K. Tang, J. Tie, and X. Li, "Covert spoofing algorithm of UAV based on GPS/INS-integrated navigation," *IEEE Trans. Veh. Technol.*, vol. 68, no. 7, pp. 6557–6564, Jul. 2019.
- [13] R. Tu, J. Liu, C. Lu, R. Zhang, P. Zhang, and X. Lu, "Cooperating the BDS, GPS, GLONASS and strong-motion observations for real-time deformation monitoring," *Geophys. J. Int.*, vol. 209, no. 3, pp. 1408–1417, Jun. 2017.

- [14] Z. Wang, W. Chen, D. Dong, C. Zhang, Y. Peng, and Z. Zheng, "An advanced multipath mitigation method based on trend surface analysis," *Remote Sens.*, vol. 12, no. 21, p. 3601, Nov. 2020.
- [15] P. Zabalegui, G. De Miguel, A. Pérez, J. Mendizabal, J. Goya, and I. Adin, "A review of the evolution of the integrity methods applied in GNSS," *IEEE Access*, vol. 8, pp. 45813–45824, 2020.
- [16] N. Zhu, J. Marais, D. Bétaille, and M. Berbineau, "GNSS position integrity in urban environments: A review of literature," *IEEE Trans. Intell. Transp. Syst.*, vol. 19, no. 9, pp. 2762–2778, Sep. 2018.
- [17] Z. Li, H. Chen, and P. Yuan, "Accelerating real-time PPP ambiguity resolution by incorporating multi-GNSS observations," *Adv. Space Res.*, vol. 63, no. 9, pp. 3009–3017, May 2019.
- [18] Z. Li, Z. Liu, and L. Zhao, "Improved robust Kalman filter for state model errors in GNSS-PPP/MEMS-IMU double state integrated navigation," *Adv. Space Res.*, vol. 67, no. 10, pp. 3156–3168, May 2021.
- [19] M. R. Kaloop, C. O. Yigit, and J. W. Hu, "Analysis of the dynamic behavior of structures using the high-rate GNSS-PPP method combined with a wavelet-neural model: Numerical simulation and experimental tests," *Adv. Space Res.*, vol. 61, no. 6, pp. 1512–1524, Mar. 2018.
- [20] H. Shen, S. Li, L. Li, W. Zhang, W. Tian, W. Hao, and R. Li, "Evaluation of ionospheric-constrained single-frequency PPP enhanced with an improved stochastic model," *Earth Sci. Informat.*, vol. 15, no. 3, pp. 1671–1681, Sep. 2022.
- [21] G. Zhang, W. Wen, B. Xu, and L.-T. Hsu, "Extending shadow matching to tightly-coupled GNSS/INS integration system," *IEEE Trans. Veh. Technol.*, vol. 69, no. 5, pp. 4979–4991, May 2020.
- [22] G. Wang, B. Cui, and C. Tang, "Robust cubature Kalman filter based on maximum correntropy and resampling-free sigma-point update framework," *Digit. Signal Process.*, vol. 126, Jun. 2022, Art. no. 103495.
- [23] Q. Zhang, Y. Hu, and X. Niu, "Required lever arm accuracy of non-holonomic constraint for land vehicle navigation," *IEEE Trans. Veh. Technol.*, vol. 69, no. 8, pp. 8305–8316, Aug. 2020.
- [24] X. Cai, H. Hsu, H. Chai, L. Ding, and Y. Wang, "Multi-antenna GNSS and INS integrated position and attitude determination without base station for land vehicles," *J. Navigat.*, vol. 72, no. 2, pp. 342–358, Mar. 2019.
- [25] M. Gerstmaier, A. Melzer, A. Onic, and M. Huemer, "On the safe road toward autonomous driving: Phase noise monitoring in radar sensors for functional safety compliance," *IEEE Signal Process. Mag.*, vol. 36, no. 5, pp. 60–70, Sep. 2019.
- [26] D. Lyu, F. Zeng, X. Ouyang, and H. Zhang, "Real-time clock comparison and monitoring with multi-GNSS precise point positioning: GPS, GLONASS and Galileo," *Adv. Space Res.*, vol. 65, no. 1, pp. 560–571, Jan. 2020.
- [27] G. Zhang and L.-T. Hsu, "Intelligent GNSS/INS integrated navigation system for a commercial UAV flight control system," *Aerosp. Sci. Technol.*, vol. 80, pp. 368–380, Sep. 2018.
- [28] P. N. Raanes, M. Bocquet, and A. Carrassi, "Adaptive covariance inflation in the ensemble Kalman filter by Gaussian scale mixtures," *Quart. J. Roy. Meteorol. Soc.*, vol. 145, no. 718, pp. 53–75, Jan. 2019.
- [29] Q. Zhang, Q. Chen, X. Niu, and C. Shi, "Requirement assessment of the relative spatial accuracy of a motion-constrained GNSS/INS in shortwave track irregularity measurement," *Sensors*, vol. 19, no. 23, p. 5296, Dec. 2019.
- [30] D. V. Cabrera, J. Utmann, and R. Förstner, "The adaptive Gaussian mixtures unscented Kalman filter for attitude determination using light curves," *Adv. Space Res.*, vol. 71, no. 6, pp. 2609–2628, Mar. 2023.
- [31] R. P. D. Vivacqua, M. Bertozzi, P. Cerri, F. N. Martins, and R. F. Vassallo, "Self-localization based on visual lane marking maps: An accurate low-cost approach for autonomous driving," *IEEE Trans. Intell. Transp. Syst.*, vol. 19, no. 2, pp. 582–597, Feb. 2018.
- [32] T. Li, H. Zhang, Z. Gao, X. Niu, and N. El-Sheimy, "Tight fusion of a monocular camera, MEMS-IMU, and single-frequency multi-GNSS RTK for precise navigation in GNSS-challenged environments," *Remote Sens.*, vol. 11, no. 6, p. 610, Mar. 2019.
- [33] A. Delépaut, P. Giordano, J. Ventura-Traveset, D. Blonski, M. Schönfeldt, P. Schoonejans, S. Aziz, and R. Walker, "Use of GNSS for lunar missions and plans for lunar in-orbit development," *Adv. Space Res.*, vol. 66, no. 12, pp. 2739–2756, Dec. 2020.
- [34] Q. Chen, Q. Zhang, and X. Niu, "Estimate the pitch and heading mounting angles of the IMU for land vehicular GNSS/INS integrated system," *IEEE Trans. Intell. Transp. Syst.*, vol. 22, no. 10, pp. 6503–6515, Oct. 2021.
- [35] H.-Q. Zhai and L.-H. Wang, "The robust residual-based adaptive estimation Kalman filter method for strap-down inertial and geomagnetic tightly integrated navigation system," *Rev. Sci. Instrum.*, vol. 91, no. 10, Oct. 2020, Art. no. 104501.
- [36] C. Xue, Y. Huang, F. Zhu, Y. Zhang, and J. A. Chambers, "An outlier-robust Kalman filter with adaptive selection of elliptically contoured distributions," *IEEE Trans. Signal Process.*, vol. 70, pp. 994–1009, 2022.
- [37] W. Li, W. Li, X. Cui, S. Zhao, and M. Lu, "A tightly coupled RTK/INS algorithm with ambiguity resolution in the position domain for ground vehicles in harsh urban environments," *Sensors*, vol. 18, no. 7, p. 2160, Jul. 2018.
- [38] M. Elsheikh, A. Noureldin, and M. Korenberg, "Integration of GNSS precise point positioning and reduced inertial sensor system for lane-level car navigation," *IEEE Trans. Intell. Transp. Syst.*, vol. 23, no. 3, pp. 2246–2261, Mar. 2022.
- [39] N. Rahemi and M. R. Mosavi, "Positioning accuracy improvement in high-speed GPS receivers using sequential extended Kalman filter," *IET Signal Process.*, vol. 15, no. 4, pp. 251–264, Jun. 2021.
- [40] D. P. Koch, D. O. Wheeler, R. W. Beard, T. W. McLain, and K. M. Brink, "Relative multiplicative extended Kalman filter for observable GPS-denied navigation," *Int. J. Robot. Res.*, vol. 39, no. 9, pp. 1085–1121, Aug. 2020.
- [41] L. Liu, S. Pan, W. Gao, C. Ma, J. Tao, and Q. Zhao, "Assessment of quad-frequency long-baseline positioning with BeiDou-3 and Galileo observations," *Remote Sens.*, vol. 13, no. 8, p. 1551, Apr. 2021.
- [42] L. Li, K. Ota, and M. Dong, "Humanlike driving: Empirical decision-making system for autonomous vehicles," *IEEE Trans. Veh. Technol.*, vol. 67, no. 8, pp. 6814–6823, Aug. 2018.
- [43] H. Zhou, J. Laval, A. Zhou, Y. Wang, W. Wu, Z. Qing, and S. Peeta, "Review of learning-based longitudinal motion planning for autonomous vehicles: Research gaps between self-driving and traffic congestion," *Transp. Res. Rec., J. Transp. Res. Board*, vol. 2676, no. 1, pp. 324–341, Jan. 2022.
- [44] D. Kong, L. Sun, and Y. Chen, "Traffic dynamics around freeway merging area with mixed conventional vehicles and connected and autonomous vehicles," *Int. J. Mod. Phys. C*, vol. 33, no. 10, Oct. 2022, Art. no. 2250128.
- [45] Q. An, S. Cheng, C. Li, L. Li, and H. Peng, "Game theory-based control strategy for trajectory following of four-wheel independently actuated autonomous vehicles," *IEEE Trans. Veh. Technol.*, vol. 70, no. 3, pp. 2196–2208, Mar. 2021.
- [46] J.-W. Shi, J.-I. Guo, M. Kagami, P. Suni, and O. Ziemann, "Photonic technologies for autonomous cars: Feature introduction," *Opt. Exp.*, vol. 27, no. 5, p. 7627, 2019.
- [47] H. Echab, A. Khallouk, and H. Ez-Zahraouy, "Effect of connected and autonomous vehicles on traffic flow at a bidirectional road," *Int. J. Mod. Phys. C*, vol. 33, no. 7, Jul. 2022, Art. no. 2250085.
- [48] X. Zhang, Z. Cheng, J. Ma, S. Huang, F. L. Lewis, and T. H. Lee, "Semi-definite relaxation-based ADMM for cooperative planning and control of connected autonomous vehicles," *IEEE Trans. Intell. Transp. Syst.*, vol. 23, no. 7, pp. 9240–9251, Jul. 2022.
- [49] C. Badue, R. Guidolini, R. V. Carneiro, P. Azevedo, V. B. Cardoso, A. Forechi, L. Jesus, R. Berriel, T. M. Paixão, F. Mutz, L. de Paula Veronese, T. Oliveira-Santos, and A. F. De Souza, "Self-driving cars: A survey," *Expert Syst. Appl.*, vol. 165, Mar. 2021, Art. no. 113816.
- [50] T. Schönberg, M. Ojala, J. Suomela, A. Torpo, and A. Halme, "Positioning an autonomous off-road vehicle by using fused DGPS and inertial navigation," *IFAC Proc. Volumes*, vol. 28, no. 11, pp. 211–216, Jun. 1995.
- [51] B. R. Hermann, A. G. Evans, C. S. Law, and B. W. Remondi, "Kinematic on-the-fly GPS positioning relative to a moving reference," *Navigation*, vol. 42, no. 3, pp. 487–501, Sep. 1995.
- [52] A. Angrisano, M. Petovello, and G. Pugliano, "GNSS/INS integration in vehicular urban navigation," in *Proc. 23rd Int. Tech. Meeting Satell. Division Inst. Navigat. (ION GNSS)*, 2010, pp. 1505–1512.
- [53] H. Liu, S. Nassar, and N. El-Sheimy, "Two-filter smoothing for accurate INS/GPS land-vehicle navigation in urban centers," *IEEE Trans. Veh. Technol.*, vol. 59, no. 9, pp. 4256–4267, Nov. 2010.
- [54] A. Lombard, X. Hao, A. Abbas-Turki, A. E. Moudni, S. Galland, and A.-U.-H. Yasar, "Lateral control of an unmanned car using GNSS positioning in the context of connected vehicles," *Proc. Comput. Sci.*, vol. 98, pp. 148–155, Jan. 2016.

- [55] H. Zhang, L. Chang, H. Wang, X. Niu, and Z. Gao, "Improvement and verification of real-time performance of GNSS/INS tightly coupled integration in embedded platform," *J. Southeast Univ., Natural Sci. Ed.*, vol. 46, no. 4, pp. 695–701, Jul. 2016.
- [56] D. Wang, Y. Dong, Q. Li, Z. Li, and J. Wu, "Using Allan variance to improve stochastic modeling for accurate GNSS/INS integrated navigation," *GPS Solutions*, vol. 22, no. 2, pp. 1–14, Apr. 2018.
- [57] D. Lyu, X. Chen, F. Wen, L. Pei, and D. He, "Urban area GNSS in-car-jammer localization based on pattern recognition," *Navigation*, vol. 66, no. 2, pp. 325–340, Jun. 2019.
- [58] Y. Ning, J. Wang, H. Han, X. Tan, and T. Liu, "An optimal radial basis function neural network enhanced adaptive robust Kalman filter for GNSS/INS integrated systems in complex urban areas," *Sensors*, vol. 18, no. 9, p. 3091, Sep. 2018.
- [59] W. Jiang, D. Liu, B. Cai, C. Rizos, J. Wang, and W. Shangquan, "A fault-tolerant tightly coupled PPP/INS/OVS integration vehicle navigation system based on an FDP algorithm," *IEEE Trans. Veh. Technol.*, vol. 68, no. 7, pp. 6365–6378, Jul. 2019.
- [60] M. Elsheikh, W. Abdelfatah, A. Noureldin, U. Iqbal, and M. Korenberg, "Low-cost real-time PPP/INS integration for automated land vehicles," *Sensors*, vol. 19, no. 22, p. 4896, Nov. 2019.
- [61] X. Li, X. Wang, J. Liao, X. Li, S. Li, and H. Lyu, "Semi-tightly coupled integration of multi-GNSS PPP and S-VINS for precise positioning in GNSS-challenged environments," *Satell. Navigat.*, vol. 2, no. 1, pp. 1–14, Dec. 2021.
- [62] K.-W. Chiang, G.-J. Tsai, H.-J. Chu, and N. El-Sheimy, "Performance enhancement of INS/GNSS/refreshed-SLAM integration for acceptable lane-level navigation accuracy," *IEEE Trans. Veh. Technol.*, vol. 69, no. 3, pp. 2463–2476, Mar. 2020.
- [63] F. Ye, S. Pan, W. Gao, H. Wang, G. Liu, C. Ma, and Y. Wang, "An improved single-epoch GNSS/INS positioning method for urban canyon environment based on real-time DISB estimation," *IEEE Access*, vol. 8, pp. 227566–227578, 2020.
- [64] Z. Yan, X. Chen, and X. Tang, "A novel linear model based on code approximation for GNSS/INS ultra-tight integration system," *Sensors*, vol. 20, no. 11, p. 3192, Jun. 2020.
- [65] S. Bijjahalli and R. Sabatini, "A high-integrity and low-cost navigation system for autonomous vehicles," *IEEE Trans. Intell. Transp. Syst.*, vol. 22, no. 1, pp. 356–369, Jan. 2021.
- [66] A. Broumandan and G. Lachapelle, "Spoofing detection using GNSS/INS/odometer coupling for vehicular navigation," *Sensors*, vol. 18, no. 5, p. 1305, Apr. 2018.
- [67] C. Ma, S. Pan, W. Gao, F. Ye, L. Liu, and H. Wang, "Improving GNSS/INS tightly coupled positioning by using BDS-3 four-frequency observations in urban environments," *Remote Sens.*, vol. 14, no. 3, p. 615, Jan. 2022.
- [68] J. Guevara, F. A. A. Cheein, J. Gené-Mola, J. R. Rosell-Polo, and E. Gregorio, "Analyzing and overcoming the effects of GNSS error on LiDAR based orchard parameters estimation," *Comput. Electron. Agricult.*, vol. 170, Mar. 2020, Art. no. 105255.
- [69] C. Zhang, X. Zhao, C. Pang, L. Zhang, and B. Feng, "The influence of satellite configuration and fault duration time on the performance of fault detection in GNSS/INS integration," *Sensors*, vol. 19, no. 9, p. 2147, May 2019.
- [70] M. Wu, J. Ding, L. Zhao, Y. Kang, and Z. Luo, "An adaptive deep-coupled GNSS/INS navigation system with hybrid pre-filter processing," *Meas. Sci. Technol.*, vol. 29, no. 2, Feb. 2018, Art. no. 025103.
- [71] B. Cui, X. Chen, X. Tang, H. Huang, and X. Liu, "Robust cubature Kalman filter for GNSS/INS with missing observations and colored measurement noise," *ISA Trans.*, vol. 72, pp. 138–146, Jan. 2018.
- [72] M. Specht, C. Specht, A. Stateczny, P. Burdziakowski, P. Dąbrowski, and O. Lewicka, "Study on the positioning accuracy of the GNSS/INS system supported by the RTK receiver for railway measurements," *Energies*, vol. 15, no. 11, p. 4094, Jun. 2022.
- [73] B. Shi, M. Wang, Y. Wang, Y. Bai, K. Lin, and F. Yang, "Effect analysis of GNSS/INS processing strategy for sufficient utilization of urban environment observations," *Sensors*, vol. 21, no. 2, p. 620, Jan. 2021.
- [74] L. Lau and P. Cross, "Development and testing of a new ray-tracing approach to GNSS carrier-phase multipath modelling," *J. Geodesy*, vol. 81, no. 11, pp. 713–732, Oct. 2007.
- [75] D. V. Ratnam, Y. Otsuka, G. Sivavaraprasad, and J. R. K. K. Dabbakuti, "Development of multivariate ionospheric TEC forecasting algorithm using linear time series model and ARMA over low-latitude GNSS station," *Adv. Space Res.*, vol. 63, no. 9, pp. 2848–2856, May 2019.
- [76] L.-T. Hsu, H. Tokura, N. Kubo, Y. Gu, and S. Kamijo, "Multiple faulty GNSS measurement exclusion based on consistency check in urban canyons," *IEEE Sensors J.*, vol. 17, no. 6, pp. 1909–1917, Mar. 2017.
- [77] C. Melendez-Pastor, R. Ruiz-Gonzalez, and J. Gomez-Gil, "A data fusion system of GNSS data and on-vehicle sensors data for improving car positioning precision in urban environments," *Expert Syst. Appl.*, vol. 80, pp. 28–38, Sep. 2017.
- [78] Z. Dai, X. Dai, Q. Zhao, Z. Bao, and C. Li, "Multi-GNSS real-time clock estimation using the dual-thread parallel method," *Adv. Space Res.*, vol. 62, no. 9, pp. 2518–2528, Nov. 2018.
- [79] W. Wen, T. Pfeifer, X. Bai, and L. Hsu, "Factor graph optimization for GNSS/INS integration: A comparison with the extended Kalman filter," *Navigation*, vol. 68, no. 2, pp. 315–331, Jun. 2021.
- [80] X. Cao, J. Li, S. Zhang, K. Kuang, K. Gao, Q. Zhao, and H. Hong, "Uncombined precise point positioning with triple-frequency GNSS signals," *Adv. Space Res.*, vol. 63, no. 9, pp. 2745–2756, May 2019.
- [81] D. Perea-Strom, A. Morell, J. Toledo, and L. Acosta, "GNSS integration in the localization system of an autonomous vehicle based on particle weighting," *IEEE Sensors J.*, vol. 20, no. 6, pp. 3314–3323, Mar. 2020.
- [82] B. Gao, G. Hu, Y. Zhong, and X. Zhu, "Cubature Kalman filter with both adaptability and robustness for tightly-coupled GNSS/INS integration," *IEEE Sensors J.*, vol. 21, no. 13, pp. 14997–15011, Jul. 2021.
- [83] F. Haque, V. Dehghanian, A. O. Fapojuwo, and J. Nielsen, "A sensor fusion-based framework for floor localization," *IEEE Sensors J.*, vol. 19, no. 2, pp. 623–631, Jan. 2019.
- [84] F. Massa, L. Bonamini, A. Settini, L. Pallottino, and D. Caporale, "LiDAR-based GNSS denied localization for autonomous racing cars," *Sensors*, vol. 20, no. 14, p. 3992, Jul. 2020.
- [85] B. Paden, M. Cáp, S. Z. Yong, D. Yershov, and E. Frazzoli, "A survey of motion planning and control techniques for self-driving urban vehicles," *IEEE Trans. Intell. Vehicles*, vol. 1, no. 1, pp. 33–55, Mar. 2016.
- [86] M. Á. de Miguel, F. García, and J. M. Armingol, "Improved LiDAR probabilistic localization for autonomous vehicles using GNSS," *Sensors*, vol. 20, no. 11, p. 3145, Jun. 2020.
- [87] A. C. B. Chiella, H. N. Machado, B. O. S. Teixeira, and G. A. S. Pereira, "GNSS/LiDAR-based navigation of an aerial robot in sparse forests," *Sensors*, vol. 19, no. 19, p. 4061, Sep. 2019.
- [88] X. Lin, F. Wang, B. Yang, and W. Zhang, "Autonomous vehicle localization with prior visual point cloud map constraints in GNSS-challenged environments," *Remote Sens.*, vol. 13, no. 3, p. 506, Jan. 2021.
- [89] P. Gao, K. Li, L. Wang, and J. Gao, "A self-calibration method for non-orthogonal angles of gimbals in tri-axis rotational inertial navigation system," *IEEE Sensors J.*, vol. 16, no. 24, pp. 8998–9005, Dec. 2016.
- [90] L. LaForest, S. M. Hasheminasab, T. Zhou, J. E. Flatt, and A. Habib, "New strategies for time delay estimation during system calibration for UAV-based GNSS/INS-assisted imaging systems," *Remote Sens.*, vol. 11, no. 15, p. 1811, Aug. 2019.
- [91] J. Kröger, T. Kersten, Y. Breva, and S. Schön, "Multi-frequency multi-GNSS receiver antenna calibration at IfE: Concept—Calibration results—Validation," *Adv. Space Res.*, vol. 68, no. 12, pp. 4932–4947, Dec. 2021.
- [92] J. Lim, W. Yoo, L. Kim, Y. Lee, and H. Lee, "Augmentation of GNSS by low-cost MEMS IMU, OBD-II, and digital altimeter for improved positioning in urban area," *Sensors*, vol. 18, no. 11, p. 3830, Nov. 2018.
- [93] A. Kaczmarek, W. Rohm, L. Klingbeil, and J. Tchórzewski, "Experimental 2D extended Kalman filter sensor fusion for low-cost GNSS/IMU/odometers precise positioning system," *Measurement*, vol. 193, Apr. 2022, Art. no. 110963.
- [94] M. M. Atia and S. L. Waslander, "Map-aided adaptive GNSS/IMU sensor fusion scheme for robust urban navigation," *Measurement*, vol. 131, pp. 615–627, Jan. 2019.
- [95] R. Ziebold, D. Medina, M. Romanovas, C. Lass, and S. Gewies, "Performance characterization of GNSS/IMU/DVL integration under real maritime jamming conditions," *Sensors*, vol. 18, no. 9, p. 2954, Sep. 2018.
- [96] B. Reuper, M. Becker, and S. Leinen, "Benefits of multi-constellation/multi-frequency GNSS in a tightly coupled GNSS/IMU/odometry integration algorithm," *Sensors*, vol. 18, no. 9, p. 3052, Sep. 2018.

- [97] L. Wang, K. Li, J. Zhang, and Z. Ding, "Soft fault diagnosis and recovery method based on model identification in rotation FOG inertial navigation system," *IEEE Sensors J.*, vol. 17, no. 17, pp. 5705–5716, Sep. 2017.
- [98] H. Qiao, M. Liu, H. Meng, M. Wang, and W. Ke, "Improved multistage in-motion attitude determination alignment method for strapdown inertial navigation system," *Sensors*, vol. 19, no. 20, p. 4568, Oct. 2019.
- [99] Y. Sun, L. Wang, Q. Cai, G. Yang, and Z. Wen, "In-motion attitude and position alignment for odometer-aided SINS based on backtracking scheme," *IEEE Access*, vol. 7, pp. 20211–20224, 2019.
- [100] G. M. Yan, J. Weng, L. Bai, and Y. Y. Qin, "Initial in-movement alignment and position determination based on inertial reference frame," *Syst. Eng. Electron.*, vol. 33, no. 3, pp. 618–621, 2011.
- [101] J. Gao, K. Li, and J. Chen, "Research on the integrated navigation technology of SINS with couple odometers for land vehicles," *Sensors*, vol. 20, no. 2, p. 546, Jan. 2020.
- [102] J. Tang, Y. Chen, X. Niu, L. Wang, L. Chen, J. Liu, C. Shi, and J. Hyypä, "LiDAR scan matching aided inertial navigation system in GNSS-denied environments," *Sensors*, vol. 15, no. 7, pp. 16710–16728, Jul. 2015.
- [103] Z. Chen, J. Lai, J. Liu, R. Li, and G. Ji, "A parameter self-calibration method for GNSS/INS deeply coupled navigation systems in highly dynamic environments," *Sensors*, vol. 18, no. 7, p. 2341, Jul. 2018.
- [104] Y. Dong, D. Wang, L. Zhang, Q. Li, and J. Wu, "Tightly coupled GNSS/INS integration with robust sequential Kalman filter for accurate vehicular navigation," *Sensors*, vol. 20, no. 2, p. 561, Jan. 2020.
- [105] C. Ma, Q. Zhang, X. Meng, N. Zheng, and S. Pan, "A novel ambiguity parameter estimation and elimination strategy for GNSS/INS tightly coupled integration," *Remote Sens.*, vol. 12, no. 21, p. 3514, Oct. 2020.
- [106] C. Wang, A. Xu, X. Sui, Y. Hao, Z. Shi, and Z. Chen, "A seamless navigation system and applications for autonomous vehicles using a tightly coupled GNSS/UWB/INS/map integration scheme," *Remote Sens.*, vol. 14, no. 1, p. 27, Dec. 2021.
- [107] S. Wang, X. Zhan, Y. Zhai, and B. Liu, "Fault detection and exclusion for tightly coupled GNSS/INS system considering fault in state prediction," *Sensors*, vol. 20, no. 3, p. 590, Jan. 2020.
- [108] Z. Zhu, C. Jiang, and Y. Bo, "Performance enhancement of GNSS/MEMS-IMU tightly integration navigation system using multiple receivers," *IEEE Access*, vol. 8, pp. 52941–52949, 2020.
- [109] C. Qian, H. Zhang, W. Li, J. Tang, H. Liu, and B. Li, "Cooperative GNSS-RTK ambiguity resolution with GNSS, INS, and LiDAR data for connected vehicles," *Remote Sens.*, vol. 12, no. 6, p. 949, Mar. 2020.
- [110] B. Hamza and A. Nebylov, "Robust nonlinear filtering applied to integrated navigation system INS/GNSS under non Gaussian measurement noise effect," *IFAC Proc. Volumes*, vol. 45, no. 1, pp. 202–207, 2012.
- [111] J. Li and Y. Wu, "Realization of GNSS/INS tightly coupled navigation and reliability verification in intelligent driving system," in *Proc. IEEE 8th Annu. Int. Conf. CYBER Technol. Autom., Control, Intell. Syst. (CYBER)*, Jul. 2018, pp. 838–842.
- [112] X. Wang, Q. Zhao, R. Xi, C. Li, G. Li, and L. Li, "Review of bridge structural health monitoring based on GNSS: From displacement monitoring to dynamic characteristic identification," *IEEE Access*, vol. 9, pp. 80043–80065, 2021.
- [113] J. Marais, J. Beugin, and M. Berbineau, "A survey of GNSS-based research and developments for the European railway signaling," *IEEE Trans. Intell. Transp. Syst.*, vol. 18, no. 10, pp. 2602–2618, Oct. 2017.



strongly interested in GNSS /INS integrated navigation signal processing.



**YUAN HE** was born in Anhui, China, in 2002. He is studying surveying and mapping engineering at Anhui Agricultural University, Hefei, China. His current research interests include GNSS/INS integrated navigation algorithms. He has collected papers on the application of GNSS/INS integrated navigation algorithms in the field of automatic driving in recent years, sorting out these papers and conducting an in-depth exploration of classic algorithms in the papers. Furthermore, he was

**JICHUAN LI** received the Ph.D. degree in signal and information processing from the Institute of Electronics, Chinese Academy of Sciences, in 2015. He is currently a Senior Engineer with the Laboratory of Science and Technology on Millimeter-Wave, Beijing Institute of Remote Sensing Equipment, China. His current research interests include missile-borne radar design, synthetic aperture radar, and adaptive space-time processing.



**JUNJIE LIU** received the master's degree in electronic science and technology from the School of Information and Electronics, Beijing Institute of Technology, in 2020. He is currently an Engineer with the Laboratory of Millimeter Wave, Beijing Institute of Remote Sensing Equipment, China. His current professional research interests include radar signal processing and remote sensing signal processing.

...